# Source time reversal (STR) method for linear elasticity

Ignacio Brevis[a,b,*], Ángel Rodríguez-Rozas[d,c], Jaime H. Ortega[a], David Pardo[c,d,e]

[a] *Departamento de Ingeniería Matemática (DIM) & Centro de Modelamiento Matemático (CMM) UMI 2807 CNRS, Universidad de Chile, Beauchef 851, Edificio Norte, Casilla 170-3, Correo 3, Santiago, Chile*

[b] *Laboratory for Scientific Image Analysis (SCIAN-Lab), BNI, Program of Anatomy and Development, ICBM, Faculty of Medicine, Universidad de Chile, Santiago, Chile*

[c] *Universidad del País Vasco (UPV/EHU), Leioa, Spain*

[d] *Basque Center for Applied Mathematics (BCAM), Bilbao, Spain*

[e] *Ikerbasque, Bilbao, Spain*

**Abstract**

We study the problem of source reconstruction for a linear elasticity problem applied to seismicity induced by mining. We assume the source is written as a variable separable function $\boldsymbol{f}(\boldsymbol{x})g(t)$. We first present a simple proof a local decay result for elasticity in the case of homogeneous media. We then extend the *source time reversal* method, originally developed for acoustic waves, to an elastic system of waves. Additionally, we present a fast reconstruction implementation for large data sets. This is especially useful in the elastic case, in which the numerical cost is higher than in fluid acoustics. We complement this work with several 2D and 3D numerical experiments and an analysis of the results.

*Keywords:* Source time reversal, time-reversal mirror, linear elasticity, induced seismicity, inverse problems
*2010 MSC:* 35R30, 65M32, 74B05

## 1. Introduction

Seismicity is described by equations of classical continuum mechanics. There are two different descriptions of motion and its mechanics: Lagrangian and Eulerian [1]. For this work, and some others seismicity applications, it is preferable to consider the Lagrangian description, which studies the displacement $\boldsymbol{u}(\boldsymbol{x}, t)$ of the particle $\boldsymbol{x}$ at time $t$. Since particle $\boldsymbol{x}$ is invariant in time, we obtain its velocity and acceleration by computing the first and second time derivatives of the displacement, respectively [1]. As there are no systematic differences between seismicity and mining seismicity (or induced seismicity) [2], it is valid to consider the same model for both seismic activities.

In this work, we are interested in applications to seismicity induced by mining. The understanding of seismic activity inside mines provides essential information to prevent

*Corresponding author
*Email addresses:* ignacio.brevis.v@gmail.com (Ignacio Brevis), angel.rodriguez.rozas@gmail.com (Ángel Rodríguez-Rozas), jortega@dim.uchile.cl (Jaime H. Ortega), dzubiaur@gmail.com (David Pardo)

accidents and improve the safety of miners. The main difference between seismicity and induced seismicity is the distance that the wavefronts travel from the source to the geophones, which in the case of induced seismicity is shorter than in seismicity. Due to this, it becomes relevant to take into account the time profile of the source in the case of induced seismicity. We propose a source of the form $\boldsymbol{f}(\boldsymbol{x})g(t)$, where $g$ is a scalar-valued function with compact support. Although considering this rather general source produces some difficulties in the reconstruction, it is physically more realistic than a traditional Dirac delta source in time. The objective is then to describe and locate the term $\boldsymbol{f}(\boldsymbol{x})$ by knowing the information provided by the geophones and $g(t)$. Geophones measure the displacement velocity by transforming the velocity of waves into voltages [3].

The problems of *source location* and *source reconstruction* have been widely studied in applied mathematics regarding their uniqueness, stability, and reconstruction. For example, V. Isakov discussed in [4] source reconstructions methods for elliptic, parabolic, and hyperbolic problems. There exist different techniques in inverse problems and control theory for solving these kinds of problems. To mention some of them, M. Yamamoto [5] in 1995 studied the problem of space-source reconstruction for the wave equation, when the source is of the form $s(\boldsymbol{x},t) = f(\boldsymbol{x})g(t)$, using exact boundary controllability and Volterra integral equations and measuring the normal derivative on the boundary. G. Garcia et al. [6] studied in 2013 a similar problem for the heat equation and reconstructed the space-term $f(\boldsymbol{x})$ from observing the solution and its time derivative in some subdomain $\mathcal{O} \subset \Omega$, where $\Omega \subset \mathbb{R}^n$ is a nonempty open bounded domain. A. El Abadia and T. Ha-Duong [7] studied in 2000 the inverse source problem for some elliptic equations from boundary measurements. They proposed an algebraic method to carry out the identifiability and also showed theoretical results. A. El Badia et al. [8] introduced on 2000 numerical results for determining a source term in elliptic problems by using the Hilbert Uniqueness Method (HUM).

In the case of wave propagation problems (including acoustics, elasticity, and electromagnetism), time reversal exploits a fundamental symmetry of waves [9]. M. Fink developed the time-reversal mirror as an extension of phase-conjugate mirrors [10], which consists of a receiver-emitter transducer device that first measures a signal, and then returns it in reversed chronology. Time-reversal mirror has applications in several areas. For example, detection of tumors and kidney stones in medical imaging, detection of defects in metals, and long-distance communication and mine detection in the ocean [11].

Time-reversal methods have also been applied for solving inverse source problems for acoustic and elastic waves. H. Ammari introduced in [12] the basis for time-reversal imaging in the context of small anomalies on the conductivity for Dirac delta sources in time and space. We mention also the works of H. Ammari et al. [13] and J. Yoo et al. [14] and their references for the state of the art for detecting small elastic anomalies.

In [15], he studies the problem of source reconstruction for the thermo-viscous model considering an attenuating acoustic media. In [16], he shows a time-reversal technique for solving inverse extended source[1] problems in the acoustic case, when the source is the derivative (in distributional sense) of a Dirac delta function in time and a smooth real-valued function with smooth compact support in space. In [17], time-reversal techniques

[1]Extended sources are those whose size is much larger than a wavelength [17].

for imaging extended source detection in elastic and viscoelastic media are presented for a source given as the derivative of a Dirac delta function in time and a vector-valued function with compact support in space. The work of H. Ammari et al. [18] shows a reconstruction of the spatial support of noisy sources in elasticity.

In [19], a method called *Source Time Reversal* (STR) was proposed for reconstructing the space term of a source of the form $f(\boldsymbol{x})g(t)$ for the acoustic wave equation. The work, with applications to mining seismicity, takes advantage of the information provided by a general time-source term $g(t)$ to transform the original source problem into an synthetic with initial conditions and without source, where the unknown $f(\boldsymbol{x})$ now appears as an initial condition for this new problem. Then, it aims to time-reverse the boundary information of the synthetic problem. Via a Volterra equation, the boundary information needed to perform the time-reversal method is obtained from the boundary measurements of the original source problem.

In the present work, we extend the STR method to the case of elasticity. This extension overcomes the difficulties encountered when considering a general time-source term. To derive this extension, we first introduce a local decay result for linear elasticity in homogeneous media. We then introduce two reconstruction methods based on different regularization terms. One of the regularizations delivers a fast reconstruction method with low computational cost. This is especially useful for large data sets, as those often appearing in elasticity. Additionally, Some 2D and 3D numerical examples are considered.

The rest of the paper is organized as follows. Section 2 describes the elasticity equation under different considerations: anisotropic, isotropic, homogeneous, and heterogeneous media. We also show some properties, behaviors, and characteristics of solutions of acoustic and elastic equations. Section 3 extends the STR method to an elastic system of waves. We then propose two reconstruction methods: the STR with traditional regularization and a fast STR with cut-off regularization. Section 4 describes two numerical implementations of the STR method, one based on the finite difference method and the other on the finite element method. In Section 5, we numerically analyze the STR with traditional regularization via 2D and 3D synthetic examples. Section 6 analyzes numerically the fast STR with cut-off regularization via more realistic 2D seismicity induced by mining examples with added noise. The last section is devoted to conclusions and future work.

## 2. Framework

In this section, we introduce some notation and review useful results of hyperbolic equations. We use bold letters to indicate vector-valued functions. Let $u : \mathbb{R}^n \to \mathbb{R}$ and $\boldsymbol{u} : \mathbb{R}^n \to \mathbb{R}^n$ be scalar-valued and vector-valued functions, respectively. Here, in the context of elastic waves $\boldsymbol{u} = (u_1, \ldots, u_n)$ stands for the displacement field, and $u_i : \mathbb{R}^n \to \mathbb{R}$ with $i \in \{1, \ldots, n\}$ corresponds to the $i$-th component of the displacement.

We denote $\Delta u$ to the Laplace operator acting on a scalar field $u$. Then, the Laplacian of a vector field is defined as

$$\Delta \boldsymbol{u} = (\Delta u_1, \ldots, \Delta u_n).$$

The curl of a vector-valued function in $\mathbb{R}^3$ is defined as

$$\operatorname{curl} \boldsymbol{u} = (\partial_{x_1}, \partial_{x_2}, \partial_{x_3}) \times (u_1, u_2, u_3) = (\partial_{x_2} u_3 - \partial_{x_3} u_2, \partial_{x_3} u_1 - \partial_{x_1} u_3, \partial_{x_1} u_2 - \partial_{x_2} u_1),$$

whereas the curl operators for a vector-valued and scalar-valued functions in $\mathbb{R}^2$ are respectively defined as

$$\operatorname{curl}_{\mathrm{v}} \boldsymbol{u} = \partial_{x_1} u_2 - \partial_{x_2} u_1 \qquad \text{and} \qquad \operatorname{curl}_{\mathrm{s}} u = (\partial_{x_2} u, -\partial_{x_1} u),$$

where we denote the curl with subscripts to differentiate both cases. Notice that $\operatorname{curl} : \mathbb{R}^3 \to \mathbb{R}^3$ in $\mathbb{R}^3$, $\operatorname{curl}_{\mathrm{v}} : \mathbb{R}^2 \to \mathbb{R}$ in $\mathbb{R}^2$, and $\operatorname{curl}_{\mathrm{s}} : \mathbb{R} \to \mathbb{R}^2$ in $\mathbb{R}^2$. Then, we have the following known properties in 3D and 2D.

**Remark 1.** *Let $\boldsymbol{u} : \mathbb{R}^3 \to \mathbb{R}^3$ be a vector-valued function and $u : \mathbb{R}^3 \to \mathbb{R}$ a scalar-valued function. Then:*

1. $\operatorname{curl} \nabla u = \mathbf{0}$.
2. $\nabla \cdot \operatorname{curl} \boldsymbol{u} = 0$.
3. $\operatorname{curl} \operatorname{curl} \boldsymbol{u} = \nabla(\nabla \cdot \boldsymbol{u}) - \Delta \boldsymbol{u}$.

**Remark 2.** *Let $\boldsymbol{u} : \mathbb{R}^2 \to \mathbb{R}^2$ be a vector-valued function and $u : \mathbb{R}^2 \to \mathbb{R}$ a scalar-valued function. Then:*

1. $\operatorname{curl}_{\mathrm{v}} \nabla u = 0$.
2. $\nabla \cdot \operatorname{curl}_{\mathrm{s}} u = 0$.
3. $\operatorname{curl}_{\mathrm{s}} \operatorname{curl}_{\mathrm{v}} \boldsymbol{u} = \nabla(\nabla \cdot \boldsymbol{u}) - \Delta \boldsymbol{u}$.
4. $\operatorname{curl}_{\mathrm{v}} \operatorname{curl}_{\mathrm{s}} u = \Delta u$.

The theory of elasticity consists of the description of stress, strain, and displacement at each point of a deformable object [20]. The general model in linear elasticity is given by the equation of motion

$$\rho \partial_t^2 \boldsymbol{u} - \nabla \cdot \underline{\underline{\sigma}}(\boldsymbol{u}) = \boldsymbol{F},$$

where $\underline{\underline{\sigma}}$ represents a second order tensor field called *stress tensor* [21]. In the isotropic case, the stress tensor takes the particular form

$$\underline{\underline{\sigma}}(\boldsymbol{u}) = \mu \left( \nabla \boldsymbol{u} + \nabla \boldsymbol{u}^T \right) + \lambda (\nabla \cdot \boldsymbol{u}) \mathrm{Id},$$

where $\mu$ and $\lambda$ are the Lamé parameters [22]. In addition, when we consider the case of homogeneous media, the tensors

$$\sigma_{ij}(\boldsymbol{u}) = \lambda \nabla \cdot \boldsymbol{u} \, \delta_{ij} + 2 \mu \, \epsilon_{ij}(\boldsymbol{u})$$

and

$$\epsilon_{ij}(\boldsymbol{u}) = \frac{1}{2} \left( \frac{\partial u_i}{\partial x_j} + \frac{\partial u_j}{\partial x_i} \right)$$

are, respectively, the classical Cauchy and stress tensors typically defined in a homogeneous and isotropic elastic media. Then, in the last case, the equation of motion is given by

$$\rho \partial_t^2 \boldsymbol{u} - \mu \Delta \boldsymbol{u} - (\mu + \lambda) \nabla (\nabla \cdot \boldsymbol{u}) = \boldsymbol{F}. \tag{1}$$

The solution $\boldsymbol{u}$ to linear elasticity is composed of two waves: the compressional and the shear wave. These waves can be written in terms of space derivatives of solutions to

acoustic problems. To do this, we consider the decomposition of the space of vector-valued square integrable functions into a direct sum of divergence-free and curl-free spaces, called *Helmholtz decomposition* [23]. In other words, let $\boldsymbol{u} \in (L^2(\mathbb{R}^n))^n$ be a vector field. Then, there exist a vector-valued function $\boldsymbol{\psi}$ and a scalar-valued function $\phi$ such that

$$\boldsymbol{u} = \boldsymbol{u}_{\text{div}} + \boldsymbol{u}_{\text{curl}}\,,$$

where $\boldsymbol{u}_{\text{div}} = \operatorname{curl} \boldsymbol{\psi}$ and $\boldsymbol{u}_{\text{curl}} = \nabla\phi$. Let us recall from Remark 1 and 2 that for the cases $n \in \{2, 3\}$, we obtain $\nabla \cdot \boldsymbol{u}_{\text{div}} = 0$ and $\operatorname{curl} \boldsymbol{u}_{\text{curl}} = \boldsymbol{0}$. We can find more general versions of this decomposition for different open sets in [24, 25].

In addition, it is easy to see by using Remarks 1 and 2 that problem (1) in 3D and 2D can be written respectively as

$$\rho\partial_t^2\boldsymbol{u} - (2\mu + \lambda)\nabla(\nabla \cdot \boldsymbol{u}) + \mu\operatorname{curl}\operatorname{curl}\boldsymbol{u} = \boldsymbol{F},$$

$$\rho\partial_t^2\boldsymbol{u} - (2\mu + \lambda)\nabla(\nabla \cdot \boldsymbol{u}) + \mu\operatorname{curl}_{\text{s}}\operatorname{curl}_{\text{v}}\boldsymbol{u} = \boldsymbol{F}.$$

In the case of homogeneous media, these expressions allow us to relate solutions of linear elasticity with acoustic solutions via the following theorems.

**Theorem 1** (Lamé's Theorem 3D case [1])**.** *Let $\boldsymbol{u}$ be the solution of the following problem*

$$\begin{cases} \rho\partial_t^2\boldsymbol{u}(\boldsymbol{x},t) - L_{\mu,\lambda}\boldsymbol{u}(\boldsymbol{x},t) = \boldsymbol{F}(\boldsymbol{x},t), & \text{in } \mathbb{R}^3 \times (0,T), \\ \boldsymbol{u}(\boldsymbol{x},0) = \nabla p(\boldsymbol{x}) + \operatorname{curl}\boldsymbol{q}(\boldsymbol{x}), \\ \partial_t\boldsymbol{u}(\boldsymbol{x},0) = \nabla r(\boldsymbol{x}) + \operatorname{curl}\boldsymbol{s}(\boldsymbol{x}), \end{cases}$$

*where $L_{\mu,\lambda}\boldsymbol{u} = (2\mu + \lambda)\nabla(\nabla \cdot \boldsymbol{u}) - \mu\operatorname{curl}\operatorname{curl}\boldsymbol{u}$, $\boldsymbol{F} = \nabla\Phi + \operatorname{curl}\boldsymbol{\Psi}$, with*

$$\nabla \cdot \boldsymbol{s} = \nabla \cdot \boldsymbol{q} = \nabla \cdot \boldsymbol{\Psi} = 0.$$

*Then, there exist functions $\phi$ and $\boldsymbol{\psi}$ such that*

$$\boldsymbol{u} = \nabla\phi + \operatorname{curl}\boldsymbol{\psi},$$

$$\nabla \cdot \boldsymbol{\psi} = 0,$$

$$\begin{cases} \partial_t^2\phi - \dfrac{\lambda + 2\mu}{\rho}\Delta\phi = \dfrac{\Phi}{\rho}, & \text{in } \mathbb{R}^3 \times (0,T), \\ \phi(\boldsymbol{x},0) = p(\boldsymbol{x}), \\ \partial_t\phi(\boldsymbol{x},0) = r(\boldsymbol{x}), \end{cases}$$

$$\begin{cases} \partial_t^2\boldsymbol{\psi} - \dfrac{\mu}{\rho}\Delta\boldsymbol{\psi} = \dfrac{\boldsymbol{\Psi}}{\rho}, & \text{in } \mathbb{R}^3 \times (0,T), \\ \boldsymbol{\psi}(\boldsymbol{x},0) = \boldsymbol{q}(\boldsymbol{x}), \\ \partial_t\boldsymbol{\psi}(\boldsymbol{x},0) = \boldsymbol{s}(\boldsymbol{x}), \end{cases}$$

*where $\nabla\phi$ and $\operatorname{curl}\boldsymbol{\psi}$ are the P-wave and S-wave, respectively, components of $\boldsymbol{u}$.*

**Theorem 2** (Lamé's Theorem 2D case [1]). *Let $\boldsymbol{u}$ be the solution of the following problem*

$$\begin{cases} \rho\partial_t^2\boldsymbol{u}(\boldsymbol{x},t) - L_{\mu,\lambda}\boldsymbol{u}(\boldsymbol{x},t) = \boldsymbol{F}(\boldsymbol{x},t), & \text{in } \mathbb{R}^2\times(0,T),\\ \boldsymbol{u}(\boldsymbol{x},0) = \nabla p(\boldsymbol{x}) + \operatorname{curl}_{\mathrm{s}} q(\boldsymbol{x}),\\ \partial_t\boldsymbol{u}(\boldsymbol{x},0) = \nabla r(\boldsymbol{x}) + \operatorname{curl}_{\mathrm{s}} s(\boldsymbol{x}), \end{cases}$$

*where $L_{\mu,\lambda}\boldsymbol{u} = (2\mu+\lambda)\nabla(\nabla\cdot\boldsymbol{u}) - \mu\operatorname{curl}_{\mathrm{s}}\operatorname{curl}_{\mathrm{v}}\boldsymbol{u}$, $\boldsymbol{F} = \nabla\Phi + \operatorname{curl}_{\mathrm{s}}\Psi$. Then, there exist functions $\phi$ and $\psi$ such that*

$$\boldsymbol{u} = \nabla\phi + \operatorname{curl}_{\mathrm{s}}\psi,$$

$$\begin{cases} \partial_t^2\phi - \dfrac{\lambda+2\mu}{\rho}\Delta\phi = \dfrac{\Phi}{\rho}, & \text{in } \mathbb{R}^2\times(0,T),\\ \phi(\boldsymbol{x},0) = p(\boldsymbol{x}),\\ \partial_t\phi(\boldsymbol{x},0) = r(\boldsymbol{x}), \end{cases}$$

$$\begin{cases} \partial_t^2\psi - \dfrac{\mu}{\rho}\Delta\psi = \dfrac{\Psi}{\rho}, & \text{in } \mathbb{R}^2\times(0,T),\\ \psi(\boldsymbol{x},0) = q(\boldsymbol{x}),\\ \partial_t\psi(\boldsymbol{x},0) = s(\boldsymbol{x}), \end{cases}$$

*where $\nabla\phi$ and $\operatorname{curl}_{\mathrm{s}}\psi$ are the P-wave and S-wave components of $\boldsymbol{u}$, respectively.*

To apply a time reversal process to linear elasticity, it is necessary to obtain a local energy decay type result. A classical result of B. R. Vainberg [26] establishes a decay rate of the solution and all its derivatives for acoustic waves and large time under certain requirements on the propagation speed, named *non-trapping condition*.

**Definition 1** (acoustic non-trapping condition [27]). *Let $c:\mathbb{R}^n\to\mathbb{R}$ be a $C^\infty(\mathbb{R}^n)$ function. We define the Hamiltonian $H(\boldsymbol{x},\boldsymbol{\xi}) = \frac{1}{2}c^2(\boldsymbol{x})|\boldsymbol{\xi}|^2$ and the following system*

$$\begin{cases} \boldsymbol{x}_t' = \frac{\partial H}{\partial\boldsymbol{\xi}} = \boldsymbol{\xi}c^2(\boldsymbol{x}),\\ \boldsymbol{\xi}_t' = -\frac{\partial H}{\partial\boldsymbol{x}} = -\frac{1}{2}|\boldsymbol{\xi}|^2\nabla(c^2(\boldsymbol{x})),\\ \boldsymbol{x}|_{t=0} = \boldsymbol{x}_0,\\ \boldsymbol{\xi}|_{t=0} = \boldsymbol{\xi}_0,\\ H(\boldsymbol{x}_0,\boldsymbol{\xi}_0) = H_0. \end{cases} \tag{2}$$

*Solutions of (2) are called bicharacteristics, and the projection of the $\boldsymbol{x}$-components into $\mathbb{R}^n$ of a bicharacteristic is called ray. We say that $c(\boldsymbol{x})$ accomplishes the* non-trapping condition *if all rays go to infinity when $t\to\infty$.*

**Theorem 3** (Local decay for acoustic solution [27]). *Let $v$ be solution to the following problem*

$$\begin{cases} \partial_t^2 v(\boldsymbol{x},t) - c^2(\boldsymbol{x})\Delta v(\boldsymbol{x},t) = 0, & \text{in } \mathbb{R}^n\times(0,\infty),\\ v(\boldsymbol{x},0) = \varphi(\boldsymbol{x}),\\ \partial_t v(\boldsymbol{x},0) = \psi(\boldsymbol{x}), \end{cases} \tag{3}$$

*where $c(\boldsymbol{x}) > c_1 > 0$ for all $\boldsymbol{x}\in\mathbb{R}^n$. Let us assume all the heterogeneities of the medium and the initial conditions are confined to a bounded subset $\Omega\subset\mathbb{R}^n$. In addition, we*

*assume $c \in C^\infty(\mathbb{R}^n)$ accomplishes the non-trapping condition. Then, there exists $T_0 > 0$ such that the solution to problem (3) verifies $v \in C^\infty(\Omega \times (T_0, \infty))$ and*

$$\left| \frac{\partial^{|\boldsymbol{\alpha}|} v(\boldsymbol{x}, t)}{\partial t^{\alpha_0} \partial x_1^{\alpha_1} \cdots \partial x_n^{\alpha_n}} \right| \leq C\eta(t) \left( \|\varphi\|_{L^2(\Omega)} + \|\psi\|_{L^2(\Omega)} \right),$$

*for all $\boldsymbol{x} \in \Omega$, for all $t \geq T_0$, and for all $\boldsymbol{\alpha} = (\alpha_0, \alpha_1, \ldots, \alpha_n) \in \mathbb{N}^{n+1}$, where $C := C(\Omega, \boldsymbol{\alpha})$. Here*

$$\eta(t) = \begin{cases} t^{1-n-\alpha_0}, & \text{for even } n \\ e^{-\delta t}, & \text{for odd } n, \end{cases}$$

*where $\delta$ is a constant depending on $c(\boldsymbol{x})$.*

Here, we employ the local decay of acoustic wave solutions given by Theorem 3 to establish a local decay result for linear elasticity.

**Theorem 4.** *Let $\boldsymbol{u}$ be solution of the linear elasticity system in homogeneous media*

$$\begin{cases} \rho \boldsymbol{u}_{tt}(\boldsymbol{x}, t) - L_{\mu,\lambda} \boldsymbol{u}(\boldsymbol{x}, t) = \boldsymbol{0}, & \text{in } \mathbb{R}^n \times (0, T), \\ \boldsymbol{u}(\boldsymbol{x}, 0) = \nabla p(\boldsymbol{x}) + \operatorname{curl} \boldsymbol{q}(\boldsymbol{x}), \\ \partial_t \boldsymbol{u}(\boldsymbol{x}, 0) = \nabla r(\boldsymbol{x}) + \operatorname{curl} \boldsymbol{s}(\boldsymbol{x}), \end{cases} \tag{4}$$

*where $\boldsymbol{q}$ and $\boldsymbol{s}$ are vector-valued functions for $n = 3$ and scalar-valued functions for $n = 2$. In addition, here $\operatorname{curl} \boldsymbol{q}$ and $\operatorname{curl} \boldsymbol{s}$ stand for $\operatorname{curl}_{\mathrm{s}} q$ and $\operatorname{curl}_{\mathrm{s}} s$ for $n = 2$. Let $\Omega \subset \mathbb{R}^n$ be a bounded set such that the supports of $p$, $\boldsymbol{q}$, $r$, and $\boldsymbol{s}$ are contained in $\Omega$. Let $\sqrt{(\lambda + 2\mu)/\rho}$, $\sqrt{\mu/\rho}$ belong to $C^\infty(\mathbb{R}^n)$ such that $\operatorname{supp}(c^* - \sqrt{(\lambda + 2\mu)/\rho}) \cup \operatorname{supp}(c^{**} - \sqrt{\mu/\rho}) \subset \Omega$ for some constants $c^*$ and $c^{**}$, $\sqrt{(\lambda + 2\mu)/\rho} \geq c^\star > 0$ and $\sqrt{\mu/\rho} \geq c^{\star\star} > 0$ for some constants $c^\star$ and $c^{\star\star}$, and $\sqrt{(\lambda + 2\mu)/\rho}$, $\sqrt{\mu/\rho}$ accomplish the non-trapping condition.*

*Then, for any $\boldsymbol{\alpha} = (\alpha, \ldots, \alpha_n)$ there exists $\widetilde{T}$ such that we have the following estimates:*

*In the 3D case,*

$$\left| \frac{\partial^{|\boldsymbol{\alpha}|} \boldsymbol{u}(\boldsymbol{x}, t)}{\partial_t^{\alpha_0} \cdots \partial_{x_3}^{\alpha_3}} \right| \leq Ce^{-\delta t} \left( \|p\|_{L^2(\Omega)} + \|r\|_{L^2(\Omega)} + \|\boldsymbol{q}\|_{(L^2(\Omega))^3} + \|\boldsymbol{s}\|_{(L^2(\Omega))^3} \right), \quad \forall\, t > \widetilde{T},$$

*for all $\boldsymbol{x} \in \Omega$, where $C := C(\Omega, \boldsymbol{\alpha}, n)$, and $\delta := \delta(\mu, \lambda, \rho)$.*

*In the 2D case,*

$$\left| \frac{\partial^{|\boldsymbol{\alpha}|} \boldsymbol{u}(\boldsymbol{x}, t)}{\partial_t^{\alpha_0} \partial_{x_1}^{\alpha_1} \partial_{x_2}^{\alpha_2}} \right| \leq Ct^{1-n-\alpha_0} \left( \|p\|_{L^2(\Omega)} + \|r\|_{L^2(\Omega)} + \|q\|_{L^2(\Omega)} + \|s\|_{L^2(\Omega)} \right), \quad \forall\, t > \widetilde{T},$$

*for all $\boldsymbol{x} \in \Omega$, where $C := C(\Omega, \boldsymbol{\alpha}, n)$.*

*Proof.* We construct the local decay estimate for the elastic waves problem. To do this, the elastic wave is decomposed in terms of the P-wave and the S-wave, and we use the

local decay result for acoustic waves. Here, we only provide the proof for the case $n = 3$; the case $n = 2$ is analogous.

Let $\boldsymbol{u}$ be a solution to (4). Then, by Theorem 1, there exist functions $\phi$ and $\boldsymbol{\psi}$ such that

$$\boldsymbol{u}(\boldsymbol{x}, t) = \nabla\phi(\boldsymbol{x}, t) + \operatorname{curl}\boldsymbol{\psi}(\boldsymbol{x}, t), \tag{5}$$

where $\phi$ solves the problem

$$\begin{cases} \partial_t^2\phi(\boldsymbol{x}, t) - \dfrac{2\mu+\lambda}{\rho}\Delta\phi(\boldsymbol{x}, t) = 0, & \text{in } \mathbb{R}^3 \times (0, \infty), \\ \phi(\boldsymbol{x}, 0) = p(\boldsymbol{x}), \\ \partial_t\phi(\boldsymbol{x}, 0) = r(\boldsymbol{x}), \end{cases}$$

and $\boldsymbol{\psi}$ solves the problem

$$\begin{cases} \partial_t^2\boldsymbol{\psi}(\boldsymbol{x}, t) - \dfrac{\mu}{\rho}\Delta\boldsymbol{\psi}(\boldsymbol{x}, t) = \boldsymbol{0}, & \text{in } \mathbb{R}^3 \times (0, \infty), \\ \boldsymbol{\psi}(\boldsymbol{x}, 0) = \boldsymbol{q}(\boldsymbol{x}), \\ \partial_t\boldsymbol{\psi}(\boldsymbol{x}, 0) = \boldsymbol{s}(\boldsymbol{x}). \end{cases}$$

Using Theorem 3, we observe that there exist $T_i$, $i \in \{0, 1, 2, 3\}$ such that

$$\begin{aligned} \left|\frac{\partial^{|\boldsymbol{\alpha}|}\phi(\boldsymbol{x}, t)}{\partial t^{\alpha_0}\partial x_1^{\alpha_1}\partial x_2^{\alpha_2}\partial x_3^{\alpha_3}}\right| &\le C_0 e^{-\delta_1 t}\left(\|p\|_{L^2} + \|r\|_{L^2}\right), && \forall\, t \ge T_0, \\ \left|\frac{\partial^{|\boldsymbol{\alpha}|}\psi_i(\boldsymbol{x}, t)}{\partial t^{\alpha_0}\partial x_1^{\alpha_1}\partial x_2^{\alpha_2}\partial x_3^{\alpha_3}}\right| &\le C_i e^{-\delta_2 t}\left(\|q_i\|_{L^2(\Omega)} + \|s_i\|_{L^2(\Omega)}\right), && \forall\, t \ge T_i, \quad i \in \{1, 2, 3\}, \end{aligned}$$

for all $\boldsymbol{x} \in \Omega$ and for all $\boldsymbol{\alpha} = (\alpha_0, \ldots, \alpha_3) \in \mathbb{N}^4$, where $C_k := C_k(\Omega, \boldsymbol{\alpha})$, with $k \in \{0, 1, 2, 3\}$, $\delta_1 := \delta_1(\rho, \mu, \lambda)$, and $\delta_2 := \delta_2(\rho, \mu)$.

From (5), we obtain the components of $\boldsymbol{u}$ in terms of $\phi$ and $\boldsymbol{\psi}$

$$\begin{aligned} u_1 &= \partial_{x_1}\phi + \partial_{x_2}\psi_3 - \partial_{x_3}\psi_2, \\ u_2 &= \partial_{x_2}\phi + \partial_{x_3}\psi_1 - \partial_{x_1}\psi_3, \\ u_3 &= \partial_{x_3}\phi + \partial_{x_1}\psi_2 - \partial_{x_2}\psi_1. \end{aligned}$$

Let $\boldsymbol{\alpha}_{+l} := (\alpha_i + \delta_{l,i})_{i=0,\ldots,n}$, where $\delta_{l,i}$ is the Kronecker delta. Then, for all $i \in \{1, 2, 3\}$

$$\begin{aligned} \left|\frac{\partial^{|\boldsymbol{\alpha}|}u_i(\boldsymbol{x}, t)}{\partial_t^{\alpha_0}\cdots\partial_{x_3}^{\alpha_3}}\right| \le& \left|\frac{\partial^{|\boldsymbol{\alpha}|+1}\phi(\boldsymbol{x}, t)}{\partial_{x_i}\partial_t^{\alpha_0}\cdots\partial_{x_3}^{\alpha_3}}\right| + \left|\frac{\partial^{|\boldsymbol{\alpha}|+1}\psi_j(\boldsymbol{x}, t)}{\partial_{x_k}\partial_t^{\alpha_0}\cdots\partial_{x_3}^{\alpha_3}}\right| + \left|\frac{\partial^{|\boldsymbol{\alpha}|+1}\psi_k(\boldsymbol{x}, t)}{\partial_{x_j}\partial_t^{\alpha_0}\cdots\partial_{x_3}^{\alpha_3}}\right| \\ \le& \widetilde{C}_1 e^{-\delta_1 t}\left(\|p\|_{L^2(\Omega)} + \|r\|_{L^2(\Omega)}\right) + \widetilde{C}_2 e^{-\delta_2 t}\left(\|q_j\|_{L^2(\Omega)} + \|s_j\|_{L^2(\Omega)}\right) \\ &+ \widetilde{C}_3 e^{-\delta_2 t}\left(\|q_k\|_{L^2(\Omega)} + \|s_k\|_{L^2(\Omega)}\right), \end{aligned}$$

where $j \ne k$, with $j, k \in \{1, 2, 3\} \setminus \{i\}$, $\delta_1 := \delta_1(\mu, \lambda, \rho)$, $\delta_2 := \delta_2(\mu, \rho)$, $\widetilde{C}_1 := \widetilde{C}_1(\Omega, \boldsymbol{\alpha}_{+i})$, $\widetilde{C}_2 := \widetilde{C}_2(\Omega, \boldsymbol{\alpha}_{+j})$, and $\widetilde{C}_3 := \widetilde{C}_3(\Omega, \boldsymbol{\alpha}_{+k})$. Let us define $\delta := \min_{l\in\{1,2\}}\delta_l$. From here, we use $C$ to denote different constants depending on $\Omega$ and $\boldsymbol{\alpha}$ (more explicitly depending

on $\Omega$, $\boldsymbol{\alpha}_{+1}$, $\boldsymbol{\alpha}_{+2}$, and $\boldsymbol{\alpha}_{+3}$). Then,

$$\begin{aligned}\left|\frac{\partial^{|\boldsymbol{\alpha}|}u_i(\boldsymbol{x},t)}{\partial_t^{\alpha_0}\cdots\partial_{x_3}^{\alpha_3}}\right| \leq & C(\Omega,\boldsymbol{\alpha})e^{-\delta t}\left(\|p\|_{L^2(\Omega)}+\|r\|_{L^2(\Omega)}+\|q_j\|_{L^2(\Omega)}+\|s_j\|_{L^2(\Omega)}\right.\\ & \left.+\|q_k\|_{L^2(\Omega)}+\|s_k\|_{L^2(\Omega)}\right)\\ \leq & C(\Omega,\boldsymbol{\alpha})e^{-\delta t}\left(\|p\|_{L^2(\Omega)}+\|r\|_{L^2(\Omega)}+\sum_{l=1}^{3}\left(\|q_l\|_{L^2(\Omega)}+\|s_l\|_{L^2(\Omega)}\right)\right)\\ \leq & C(\Omega,\boldsymbol{\alpha})e^{-\delta t}\left(\|p\|_{L^2(\Omega)}+\|r\|_{L^2(\Omega)}+\sqrt{3}\left(\|\boldsymbol{q}\|_{(L^2(\Omega))^3}+\|\boldsymbol{s}\|_{(L^2(\Omega))^3}\right)\right)\\ \leq & C(\Omega,\boldsymbol{\alpha},n)e^{-\delta t}\left(\|p\|_{L^2(\Omega)}+\|r\|_{L^2(\Omega)}+\|\boldsymbol{q}\|_{(L^2(\Omega))^3}+\|\boldsymbol{s}\|_{(L^2(\Omega))^3}\right).\end{aligned}$$

Note that constant $C$ depends on $n$ in this last estimate. On the other hand,

$$\begin{aligned}\left|\frac{\partial^{|\boldsymbol{\alpha}|}\boldsymbol{u}(\boldsymbol{x},t)}{\partial_t^{\alpha_0}\cdots\partial_{x_3}^{\alpha_3}}\right| = & \sqrt{\left|\frac{\partial^{|\boldsymbol{\alpha}|}u_1(\boldsymbol{x},t)}{\partial_t^{\alpha_0}\cdots\partial_{x_3}^{\alpha_3}}\right|^2+\left|\frac{\partial^{|\boldsymbol{\alpha}|}u_2(\boldsymbol{x},t)}{\partial_t^{\alpha_0}\cdots\partial_{x_3}^{\alpha_3}}\right|^2+\left|\frac{\partial^{|\boldsymbol{\alpha}|}u_3(\boldsymbol{x},t)}{\partial_t^{\alpha_0}\cdots\partial_{x_3}^{\alpha_3}}\right|^2}\\ \leq & \left|\frac{\partial^{|\boldsymbol{\alpha}|}u_1(\boldsymbol{x},t)}{\partial_t^{\alpha_0}\cdots\partial_{x_3}^{\alpha_3}}\right|+\left|\frac{\partial^{|\boldsymbol{\alpha}|}u_2(\boldsymbol{x},t)}{\partial_t^{\alpha_0}\cdots\partial_{x_3}^{\alpha_3}}\right|+\left|\frac{\partial^{|\boldsymbol{\alpha}|}u_3(\boldsymbol{x},t)}{\partial_t^{\alpha_0}\cdots\partial_{x_3}^{\alpha_3}}\right|\\ \leq & C(\Omega,\boldsymbol{\alpha},n)e^{-\delta t}\left(\|p\|_{L^2(\Omega)}+\|r\|_{L^2(\Omega)}+\|\boldsymbol{q}\|_{(L^2(\Omega))^3}+\|\boldsymbol{s}\|_{(L^2(\Omega))^3}\right).\end{aligned}$$

Then,

$$\left|\frac{\partial^{|\boldsymbol{\alpha}|}\boldsymbol{u}(\boldsymbol{x},t)}{\partial_t^{\alpha_0}\partial_{x_1}^{\alpha_1}\partial_{x_2}^{\alpha_2}\partial_{x_3}^{\alpha_3}}\right| \leq Ce^{-\delta t}\left(\|p\|_{L^2(\Omega)}+\|r\|_{L^2(\Omega)}+\|\boldsymbol{q}\|_{(L^2(\Omega))^3}+\|\boldsymbol{s}\|_{(L^2(\Omega))^3}\right),$$

for all $t>\widetilde{T}$, $\boldsymbol{x}\in\Omega$ and for all $\boldsymbol{\alpha}=(\alpha_0,\alpha_1,\alpha_2,\alpha_3)\in\mathbb{N}^4$, where $\widetilde{T}=\max\{T_0,\ldots,T_3\}$. This proves the theorem in the case $n=3$.

The same proof remains valid in the 2D case by considering $\boldsymbol{\psi}$, $\boldsymbol{q}$, and $\boldsymbol{s}$ as scalar valued functions, so we obtain

$$\left|\frac{\partial^{|\boldsymbol{\alpha}|}u_i(\boldsymbol{x},t)}{\partial_t^{\alpha_0}\partial_{x_1}^{\alpha_1}\partial_{x_2}^{\alpha_2}}\right| \leq Ct^{1-n-\alpha_0}\left(\|p\|_{L^2(\Omega)}+\|q\|_{L^2(\Omega)}+\|r\|_{L^2(\Omega)}+\|s\|_{L^2(\Omega)}\right),$$

for all $t>\widetilde{T}$, $\boldsymbol{x}\in\Omega$, and for all $\boldsymbol{\alpha}=(\alpha_0,\alpha_1,\alpha_2)\in\mathbb{N}^3$, where $\widetilde{T}=\max\{T_0,T_1\}$. This completes the proof. □

## 3. Source time reversal in elasticity

STR [19] method modifies the classical Time-Reversal Mirrors (TRM) [28] for reconstructing a space-source term of the form $s(\boldsymbol{x},t)=f(\boldsymbol{x})g(t)$, where $g$ is a real-valued function with compact support. Taking advantage of the information provided by the time-source term $g(t)$, the original source problem is related with a non-source wave problem in which the space-source term of the original problem appears as an initial condition and the boundaries information between the two problems are related by a Volterra integral equation of the first kind. Then, it is possible to apply the TRM idea over this new non-source initial condition problem by solving the integral equation to

obtain its boundary information and chronologically reverse the boundary information of the non-source wave problem.

Although acoustics provide a good first approximation of compressional and shear waves, linear elasticity offers a better approximation to the ground motion. In [29], we can see the main limitations of considering the acoustic model for seismic events. Since STR method is oriented to solve problems in induced seismicity, in here we extend the original formulation for acoustic waves [19] to systems of elastic waves.

In this section, we select a model for tremors by considering compressional and shear waves propagating in an infinite medium (without boundary). Assuming our seismic events are governed by the elastic equation in an isotropic media, we use the Lagrangian description [1] to define the displacement $\boldsymbol{u}(\boldsymbol{x},t)$ of the particle $\boldsymbol{x}$ at time $t$ in an homogeneous and isotropic elastic media

$$\begin{cases} \rho\partial_t^2\boldsymbol{u}(\boldsymbol{x},t) - L_{\mu,\lambda}\boldsymbol{u}(\boldsymbol{x},t) = \boldsymbol{f}(\boldsymbol{x})g(t), & \text{in } \mathbb{R}^n \times (0,T), \\ \boldsymbol{u}(\boldsymbol{x},0) = \boldsymbol{0}, \\ \partial_t\boldsymbol{u}(\boldsymbol{x},0) = \boldsymbol{0}, \end{cases} \tag{6}$$

where $L_{\mu,\lambda}\boldsymbol{u} = \mu\Delta\boldsymbol{u} + (\mu+\lambda)\nabla(\nabla\cdot\boldsymbol{u})$ and $n \in \{2,3\}$.

Let us consider a bounded set $\Omega \subset \mathbb{R}^n$ such that the support of $\boldsymbol{f}(\boldsymbol{x})$ is contained in $\Omega$, and the geophones are located on $\partial\Omega$. The boundary information will be given by the displacement velocities $\partial_t\boldsymbol{u}(\boldsymbol{y},t)$ for $\boldsymbol{y} \in \partial\Omega$ and for all $t \in (0,T)$. Then, we define the inverse problem: given the measurement displacement velocities $\{m_{\boldsymbol{u}}(\boldsymbol{y},t) := \partial_t\boldsymbol{u}(\boldsymbol{y},t) : (\boldsymbol{y},t) \in \partial\Omega \times (0,T)\}$ and the time-distribution of the source $\{g(t) : t \in (0,T)\}$, find the space-source term $\boldsymbol{f}(\boldsymbol{x})$. We introduce the operator of measurement displacement velocities as

$$\Lambda(\boldsymbol{f},g) := \partial_t\boldsymbol{u}|_{\partial\Omega\times(0,T)}.$$

We define an initial condition problem by following the procedure in [19]

$$\begin{cases} \rho\partial_t^2\boldsymbol{v}(\boldsymbol{x},t) - L_{\mu,\lambda}\boldsymbol{v}(\boldsymbol{x},t) = \boldsymbol{0}, & \text{in } \mathbb{R}^n \times (0,T), \\ \boldsymbol{v}(\boldsymbol{x},0) = \boldsymbol{0}, \\ \partial_t\boldsymbol{v}(\boldsymbol{x},0) = \rho^{-1}\boldsymbol{f}(\boldsymbol{x}), \end{cases} \tag{7}$$

where the solutions to (6) and (7) are related via an integral equation by using Duhamel's principle [30]

$$\boldsymbol{u}(\boldsymbol{x},t) = \int_0^t \boldsymbol{v}(\boldsymbol{x},t-\tau)g(\tau)\,dt. \tag{8}$$

We are interested in obtaining the boundary measurements from problem (7) in order to reverse them chronologically and recover $\boldsymbol{f}(\boldsymbol{x})$. To do this, we define the operator of measurements

$$\Lambda_0\boldsymbol{f} := \partial_t\boldsymbol{v}|_{\partial\Omega\times(0,T)}.$$

Notice that it is possible to rewrite problem (7) inside $\Omega$ in terms of the displacement velocity, the boundary information and its conditions at time $t = T$. Then, the solution

to problem (9) is the restriction of $\partial_t \boldsymbol{v}(\boldsymbol{x},t)$ inside $\Omega \times (0,T]$.

$$\begin{cases} \rho\partial_t^2 \boldsymbol{w}(\boldsymbol{x},t) - L_{\mu,\lambda}\boldsymbol{w}(\boldsymbol{x},t) = \boldsymbol{0}, & \text{in } \Omega \times (0,T), \\ \boldsymbol{w}(\boldsymbol{x},T) = \partial_t \boldsymbol{v}(\boldsymbol{x},T), & \\ \partial_t \boldsymbol{w}(\boldsymbol{x},T) = \partial_t^2 \boldsymbol{v}(\boldsymbol{x},T), & \\ \boldsymbol{w}(\boldsymbol{y},t) = m_{\boldsymbol{v}}(\boldsymbol{y},t), & \text{on } \partial\Omega \times (0,T), \end{cases} \tag{9}$$

where $m_{\boldsymbol{v}} := \Lambda_0 \boldsymbol{f}$.

To obtain the solution to problem (9) at time $t = 0$ is equivalent to back propagate the displacement velocity waves in problem (7). This procedure gives us an exact reconstruction of the initial velocity to problem (7), i.e. $\boldsymbol{w}(\boldsymbol{x},0) = \rho^{-1}\boldsymbol{f}(\boldsymbol{x})$. Unfortunately, the final conditions $\partial_t \boldsymbol{v}(\boldsymbol{x},T)$ and $\partial_t^2 \boldsymbol{v}(\boldsymbol{x},T)$ for all $\boldsymbol{x} \in \Omega$ are often unavailable in a practical setting. To overcome this issue, we notice from Theorem 4 that not only each component of the solution of (7) decays, but also its derivatives inside the bounded set $\Omega$ for large $T$. Furthermore, the decay profile is polynomial in 2D and exponential in 3D. Thus, the final conditions $\partial_t \boldsymbol{v}(\boldsymbol{x},T)$ and $\partial_t^2 \boldsymbol{v}(\boldsymbol{x},T)$ to problem (9) can be approximated by zero for $T$ large enough.

Let us assume that problem (7) satisfies the conditions of Theorem 4 and let $T - \varepsilon > \widetilde{T}$ for a fixed $\varepsilon > 0$. Then, we define the following problem

$$\begin{cases} \rho\partial_t^2 \widetilde{\boldsymbol{w}} - L_{\mu,\lambda}\widetilde{\boldsymbol{w}} = \boldsymbol{0}, & \text{in } \Omega \times (0,T), \\ \widetilde{\boldsymbol{w}}(\boldsymbol{x},T) = \boldsymbol{0}, & \\ \partial_t \widetilde{\boldsymbol{w}}(\boldsymbol{x},T) = \boldsymbol{0}, & \\ \widetilde{\boldsymbol{w}}(\boldsymbol{y},t) = m_{\boldsymbol{v}}(\boldsymbol{y},t)\phi_\varepsilon(t), & \text{on } \partial\Omega \times (0,T), \end{cases} \tag{10}$$

where $\phi_\varepsilon$ is a smooth cut-off function such that $\phi_\varepsilon(t) = 1$ for all $t \in (0, T-\varepsilon)$ and $\phi_\varepsilon = 0$ for all $t \in (T, \infty)$. By solving problem (10) at time $t = 0$, we obtain an approximate reconstruction of $\rho^{-1}\boldsymbol{f}(\boldsymbol{x})$. This reconstruction depends mainly on $T$ and the dimension of the problem $n$.

From the physical problem (6), we measure the boundary information denoted by the set $\{m_{\boldsymbol{u}}(\boldsymbol{y},t) = \partial_t \boldsymbol{u}(\boldsymbol{y},t) : (\boldsymbol{y},t) \in \partial\Omega \times (0,T)\}$. To solve problem (10), it is necessary to obtain the boundary information from the synthetic problem (7) given by the set $\{m_{\boldsymbol{v}}(\boldsymbol{y},t) = \partial_t \boldsymbol{v}(\boldsymbol{y},t) : (\boldsymbol{y},t) \in \partial\Omega \times (0,T)\}$. Then, it only remains to obtain the measurements $m_{\boldsymbol{v}}(\boldsymbol{y},\cdot)$ from $m_{\boldsymbol{u}}(\boldsymbol{y},\cdot)$ for each $\boldsymbol{y} \in \partial\Omega$. From identity (8), this problem reduces to solve the following integral equation

$$m_{\boldsymbol{u}}(\boldsymbol{y},t) = \int_0^t m_{\boldsymbol{v}}(\boldsymbol{y},t-\tau)g(\tau)\,dt, \tag{11}$$

where $t \in (0,T)$ for all $\boldsymbol{y} \in \partial\Omega$.

Let $\mathcal{A}_0(m_{\boldsymbol{u}}, g) = m_{\boldsymbol{v}}$ be the operator that solves problem (11). Then, we need to solve the following problem to obtain a reconstruction to the space-source term $\boldsymbol{f}(\boldsymbol{x})$

$$\begin{cases} \rho\partial_t^2 \widetilde{\boldsymbol{w}} - L_{\mu,\lambda}\widetilde{\boldsymbol{w}} = \boldsymbol{0}, & \text{in } \Omega \times (0,T), \\ \widetilde{\boldsymbol{w}}(\boldsymbol{x},T) = \boldsymbol{0}, & \\ \partial_t \widetilde{\boldsymbol{w}}(\boldsymbol{x},T) = \boldsymbol{0}, & \\ \widetilde{\boldsymbol{w}}(\boldsymbol{y},t) = \rho\mathcal{A}_0(m_{\boldsymbol{u}}, g)(\boldsymbol{y},t)\phi_\varepsilon(t), & \text{on } \partial\Omega \times (0,T). \end{cases} \tag{12}$$

The Laplace transform is a standard tool to solve integral equations of the first kind when the kernel is given by a convolution. A limitation of this technique is that the inverse Laplace transform is known only for some rather simple functions and it may also be challenging to find numerically [31].

To overcome the above limitation, we propose to solve (11) numerically by using Fourier transform. Unfortunately, a direct resolution gives us the expression

$$\mathcal{F}^{-1}\left(\frac{\mathcal{F}(m_{\boldsymbol{u}})}{\mathcal{F}(g)}\right),$$

which may become singular for some $t$ and it is numerically unstable. To avoid the previous stability problems, we present two regularization methods for approximating the solution to (11).

*STR with traditional regularization.* We define

$$\mathcal{A}(m_{\boldsymbol{u}}, g) := \mathcal{F}^{-1}\left(\frac{\mathcal{F}(m_{\boldsymbol{u}})\overline{\mathcal{F}(g)}}{|\mathcal{F}(g)|^2 + c_0}\right), \tag{13}$$

where $c_0$ is a small positive regularization constant. Then, we replace the operator $\mathcal{A}_0$ with $\mathcal{A}$ in problem (12) to find a reconstruction of the space-source term $\boldsymbol{f}(\boldsymbol{x})$.

With the above regularization, high frequencies appear due to the division by $F(g)$. This regularization method was considered in [19]. The addition of the constant $c_0$ makes the deconvolution stable and avoids divisions by zero but does not eliminate high frequencies. Solving such high frequencies require the use of fine meshes in numerical simulations. For large problems, the method may eventually become prohibitively expensive.

*Fast STR with cut-off regularization.* In this second regularization method, we define function $\Theta$ as

$$\Theta(\xi) = \begin{cases} \dfrac{\overline{\mathcal{F}(g)(\xi)}}{|\mathcal{F}(g)(\xi)|^2}, & \text{if } |\mathcal{F}(g)(\xi)| \geq c_1 \max\limits_{\xi} |\mathcal{F}(g)(\xi)| \\ 0, & \text{if } |\mathcal{F}(g)(\xi)| < c_1 \max\limits_{\xi} |F(g)(\xi)|, \end{cases}$$

where $c_1 \in (0, 1)$ is a constant that regulates excitations of high frequencies and avoids divisions by zero. Then, we replace the operator $\mathcal{A}_0$ with

$$\mathcal{F}^{-1}(\mathcal{F}(m_{\boldsymbol{u}})\Theta) \tag{14}$$

in problem (12) to find a reconstruction of the source-space term $\boldsymbol{f}(\boldsymbol{x})$. This regularization method allows the source reconstruction in coarse meshes by eliminating higher frequencies.

In summary, the STR method consists of a transformation of the boundary measurements, which are given by the displacement velocities. To transform the boundary measurements, we propose two regularization methods depending on the computational requirements. The first one reverses in time the measurements processed by operator $\mathcal{A}$ to recover the space-source term. The second regularization method eliminates high frequencies of the processed signals to be reversed in time. This second approach allows

for reconstructing sources in more realistic cases when the computational requirements are larger. Figure 1 shows the difference in the processed signal frequencies between the two regularization methods for different regularization constants. Both procedures will give us a reconstruction of $\boldsymbol{f}(\boldsymbol{x})$ for any time-source term $g(t)$.

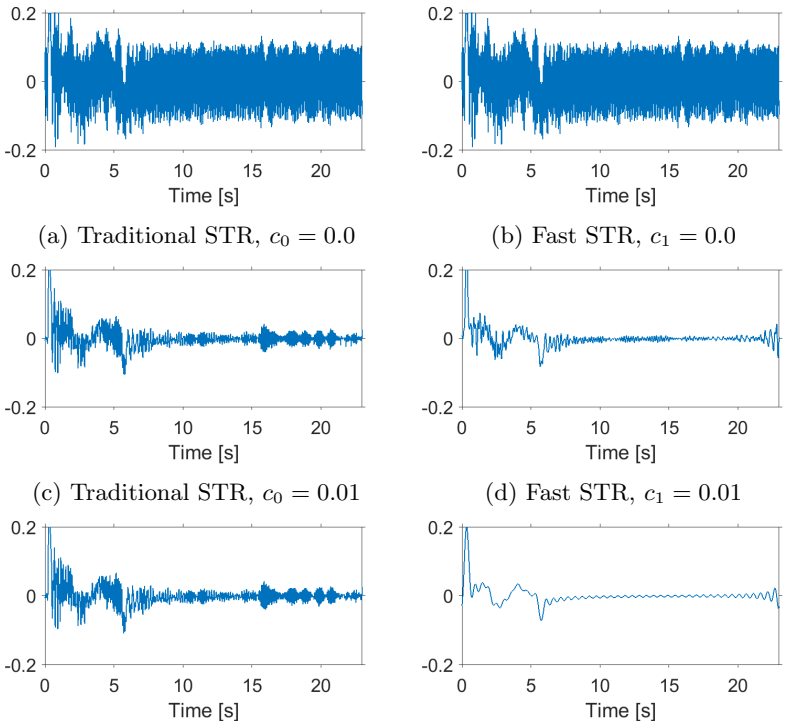


(a) Traditional STR, $c_0 = 0.0$ (b) Fast STR, $c_1 = 0.0$

(c) Traditional STR, $c_0 = 0.01$ (d) Fast STR, $c_1 = 0.01$

(e) Traditional STR, $c_0 = 0.1$ (f) Fast STR, $c_1 = 0.1$

Figure 1: First component of a measurement processed with both STR regularization methods for different regularization constant values.

## 4. Implementation of the STR method

We consider two simulation methods: a Finite Difference Method (FDM) and a Finite Element Method (FEM). In the absence of analytical solutions, we use both schemes to compare our results and validate the robustness of the method.

The implementation considered for the FDM is straightforward and based on the 2D scheme presented in [32]. Then, the 2D system $(u, v)$ governed by

$$\begin{aligned} \rho \frac{\partial^2 u}{\partial t^2} &= (2\mu + \lambda) \frac{\partial}{\partial x} \left( \frac{\partial u}{\partial x} + \frac{\partial v}{\partial y} \right) + \mu \frac{\partial}{\partial y} \left( \frac{\partial u}{\partial y} - \frac{\partial v}{\partial x} \right), \\ \rho \frac{\partial^2 v}{\partial t^2} &= \mu \frac{\partial}{\partial x} \left( \frac{\partial v}{\partial x} - \frac{\partial u}{\partial y} \right) + (2\mu + \lambda) \frac{\partial}{\partial y} \left( \frac{\partial u}{\partial x} + \frac{\partial v}{\partial y} \right), \end{aligned}$$

is discretized as follows:

$$U_{l+1}(i,j) = 2U_l(i,j) - U_{l-1}(i,j) + \left(\frac{v_p \Delta t}{h}\right)^2 [U_l(i+1,j) - 2U_l(i,j) + U_l(i-1,j)]$$
$$+ \left(\frac{v_p \Delta t}{h}\right)^2 \left(1 - \frac{v_s}{v_p}\right) [V_l(i+1,j+1) - V_l(i+1,j-1) - V_l(i-1,j+1)$$
$$+ V_l(i-1,j-1)]/4 + \left(\frac{v_p \Delta t}{h}\right)^2 \left(\frac{v_s}{v_p}\right)^2 [U_l(i,j+1) - 2U_l(i,j) + U_l(i,j-1)] ,$$

$$V_{l+1}(i,j) = 2V_l(i,j) - V_{l-1}(i,j) + \left(\frac{v_p \Delta t}{h}\right)^2 [V_l(i,j+1) - 2V_l(i,j) + V_l(i,j-1)]$$
$$+ \left(\frac{v_p \Delta t}{h}\right)^2 \left(1 - \frac{v_s}{v_p}\right) [U_l(i+1,j+1) - U_l(i+1,j-1) - U_l(i-1,j+1)$$
$$+ U_l(i-1,j-1)]/4 + \left(\frac{v_p \Delta t}{h}\right)^2 \left(\frac{v_s}{v_p}\right)^2 [V_l(i+1,j) - 2V_l(i,j) + V_l(i-1,j)] ,$$

where $(U_{l+1} - 2U_l + U_{l-1})/(\Delta t)^2$ is the finite difference discretization for $\partial^2 u/\partial t^2$ at time $t = l\Delta t$, $\Delta t$ is the time discretization step, $h$ is the space discretization step, $v_p = \sqrt{(2\mu + \lambda)/\rho}$, and $v_s = \sqrt{\mu/\rho}$. Additionally, in here we extend this scheme to the 3D case, where the system $(u, v, w)$ is given by

$$\rho \frac{\partial^2 u}{\partial t^2} = (2\mu + \lambda) \frac{\partial}{\partial x}\left(\frac{\partial u}{\partial x} + \frac{\partial v}{\partial y} + \frac{\partial w}{\partial z}\right) + \mu \frac{\partial}{\partial y}\left(\frac{\partial u}{\partial y} - \frac{\partial v}{\partial x}\right) + \mu \frac{\partial}{\partial z}\left(\frac{\partial u}{\partial z} - \frac{\partial w}{\partial x}\right)$$
$$\rho \frac{\partial^2 v}{\partial t^2} = \mu \frac{\partial}{\partial x}\left(\frac{\partial v}{\partial x} - \frac{\partial u}{\partial y}\right) + (2\mu + \lambda) \frac{\partial}{\partial y}\left(\frac{\partial u}{\partial x} + \frac{\partial v}{\partial y} + \frac{\partial w}{\partial z}\right) + \mu \frac{\partial}{\partial z}\left(\frac{\partial v}{\partial z} - \frac{\partial w}{\partial y}\right)$$
$$\rho \frac{\partial^2 w}{\partial t^2} = \mu \frac{\partial}{\partial x}\left(\frac{\partial w}{\partial x} - \frac{\partial u}{\partial z}\right) + \mu \frac{\partial}{\partial y}\left(\frac{\partial w}{\partial y} - \frac{\partial v}{\partial z}\right) + (2\mu + \lambda) \frac{\partial}{\partial z}\left(\frac{\partial u}{\partial x} + \frac{\partial v}{\partial y} + \frac{\partial w}{\partial z}\right)$$

For the forward problem, we consider a large enough computational domain to ensure that waves measured by the geophones are free from the effects of the computational boundary. To reverse the measurements processed by the STR method, we consider a smaller computational domain equal to $\Omega$, where the geophones are in the computational boundary of the domain. Finally, the processed signal is introduced as the Dirichlet condition of the backward problem.

For the FEM, we implemented a first-order absorbing boundary condition over the domain boundary $\Gamma \subset \Omega$:

$$\rho \frac{\partial^2 \boldsymbol{u}}{\partial t^2} - \nabla \cdot \underline{\underline{\sigma}}(\boldsymbol{u}) = g(t) \left(0.5 \nabla + 0.5 \nabla \times\right) \delta_{\boldsymbol{x}_0}, \qquad \text{in } \Omega, \tag{17a}$$
$$\rho B \frac{\partial \boldsymbol{u}}{\partial t} + \underline{\underline{\sigma}}(\boldsymbol{u}) \cdot \mathbf{n} = \mathbf{0}, \qquad \text{on } \Gamma, \tag{17b}$$

where the external force $g(t)\,(0.5\,\nabla + 0.5\,\nabla\times)\,\delta_{\boldsymbol{x}_0}$ represents a point source in space ($\delta$) located at $\boldsymbol{x}_0$ that generates both P- and S-waves, $g(t)$ is a source time function based on a Ricker wavelet with peak frequency $f_p$ (typically 10 $[Hz]$), and $\mathbf{n}$ is the exterior unit normal to the boundary $\Gamma$. Note that more point sources may be considered by simply adding similar terms to the right-hand-side at different space locations. The symmetric, positive-definite matrix $B$ appearing in the absorbing boundary condition of equation (17b) is defined as

$$B := \begin{pmatrix} c_P n_1^2 + c_S n_2^2 & (c_P - c_S) n_1 n_2 \\ (c_P - c_S) n_1 n_2 & c_P n_1^2 + c_S n_2^2 \end{pmatrix},$$

where $n_1$ and $n_2$ are the normal components in the first and second directions, respectively, and $c_P$ and $c_S$ are the compressional and the shear wave velocities, respectively, with $c_P = \sqrt{\frac{\lambda+2\mu}{\rho}}$ and $c_S = \sqrt{\frac{\mu}{\rho}}$.

The weak formulation of problem (17) reads as follows: $\forall t \in (0, T]$, find $\boldsymbol{u} = \boldsymbol{u}(t) \in U$ such that

$$\int_\Omega \rho \frac{\partial^2 \boldsymbol{u}}{\partial t^2} \cdot \mathbf{w} d\Omega + \int_\Omega \lambda\, \nabla \cdot \boldsymbol{u}\, \nabla \cdot \mathbf{w}\, d\Omega + \int_\Omega 2\mu \sum_{i,j=1}^{2} \epsilon_{i,j}(\boldsymbol{u}) \epsilon_{i,j}(\mathbf{w}) d\Omega$$

$$+ \int_\Gamma \rho \left( B \frac{\partial \boldsymbol{u}}{\partial t} \right) \cdot \mathbf{w} d\Gamma = \int_\Omega g(t)\,(0.5\,\nabla + 0.5\,\nabla\times)\,\delta_{\boldsymbol{x}_0} \cdot \mathbf{w}\, d\Omega,$$

for all test functions $\mathbf{w} \in W$, where the Sobolev trial space $U$ and test space $W$ are defined as

$$U = \{\boldsymbol{u} \in (H^1(\Omega))^2\},$$

and

$$W = \{\mathbf{w} \in (H^1(\Omega))^2 : \mathbf{w} = \mathbf{0} \text{ on } \Gamma\}.$$

We consider the Leap-frog scheme for the second-order time derivative, whereas for the first-order one we apply central differences. For the space discretization, we employ high-order hierarchical basis functions for the space discretization for both the finite-dimensional test and trial spaces $V_h$ and $W_h$. Therefore, we obtain a numerical scheme that provides second-order accuracy in time, exhibits an arbitrary convergence order in space (typically, we fix the polynomial order p to be $p = 2$ or $p = 3$), and it conserves the energy (see [33]) provided that a certain CFL condition is satisfied. This CFL condition imposes a constrained relationship between the magnitudes of the time step $\Delta t$ and the characteristic element size $h$, the later selected according to $f_p$. For a regular mesh over a rectangular domain, this CFL condition becomes

$$\Delta t < \frac{2h}{\sqrt{\alpha\, d}},$$

where $d$ is the dimension of the domain $\Omega$ (two in our case) and $\alpha$ is a constant that depends only on the space discretization method.

For the backward problem, a similar discretization holds. The only difference is that now we replace equation (17a) by its corresponding homogeneous problem and equation (17b) by a Dirichlet boundary condition on $\Gamma$ using the transformed data registered by the geophones on the forward problem, as described in the previous section.

## 5. Numerical experiments of STR with traditional regularization

In this section, we employ the FDM. We consider a source supported in a subdomain $\Omega = (-3, 3) \times (-3, 3)$ for the 2D case, and $\Omega = (-3, 3) \times (-3, 3) \times (-3, 3)$ for the 3D case. In the following experiments, we consider regular grids composed of squares (2D) or cubes (3D). Let us denote by $\partial\Omega_h$ the nodes of the numeric mesh over $\partial\Omega$. The geophones will be located at each nodal point of $\partial\Omega_h$ for the experiments with measure-ments over the entire boundary and at each point of a set $\Gamma_h \subset \partial\Omega_h$ for experiments with partial data. The measurements are processed with the operator defined in (13). In Subsections 5.1, 5.2, and 5.4, we consider the regularization constant $c_0 = 0.01$ for the standard STR. Additionally, in the last subsection, we compare both STR regularization methods (traditional and fast) for data in the entire boundary and for partial boundary information.

We consider the following elastic parameters: $\rho = 1\ [Kg/m^3]$, $\mu = 1\ [Pa]$, $\lambda = 1\ [Pa]$. Thus, the speed of the P-wave is $\sqrt{2}\ [m/s]$ and that of the S-wave is $1\ [m/s]$. We generate elastic waves by considering different sources $\boldsymbol{f}(\boldsymbol{x})g(t)$. In most of these experiments, we consider three time-source terms given by

$$g_1(t) = \frac{g_s(t)}{\|g_s(t)\|},\ g_2(t) = \begin{cases} 7t, & t \in (0, 1/7) \\ 1, & t \in (1/7, 2/7) \\ 3 - 7t, & t \in (2/7, 3/7) \end{cases},\ \text{and } g_3(t) = 1\chi_{(0.01,0.4)},$$

where $g_s(t) = \exp(1 - 12^2(t - 0.2)^2)$. Figure 2 displays these functions.

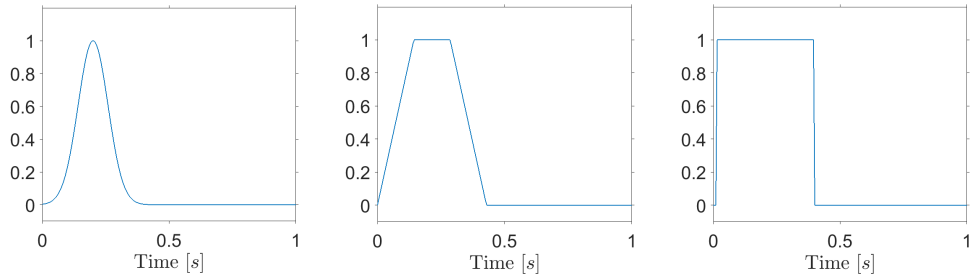


(a) $g_1(t)$ (b) $g_2(t)$ (c) $g_3(t)$

Figure 2: Time-source terms.

### 5.1. Two-dimensional phantom reconstruction

The scope of this experiment is to analyze the effect of the shape of the time source on the recovered reconstruction results for 2D simulations in an ideal case. We refer to an ideal case as an experiment without noise, with geophones located at all mesh nodes along the entire $\partial\Omega$, and a final time $T$ long enough to measure the wavefronts. To do this, we present 2D reconstructions of the known Shepp-Logan phantom [34] as the space-source term, see Figure 3a. Here, we generate the elastic waves using three

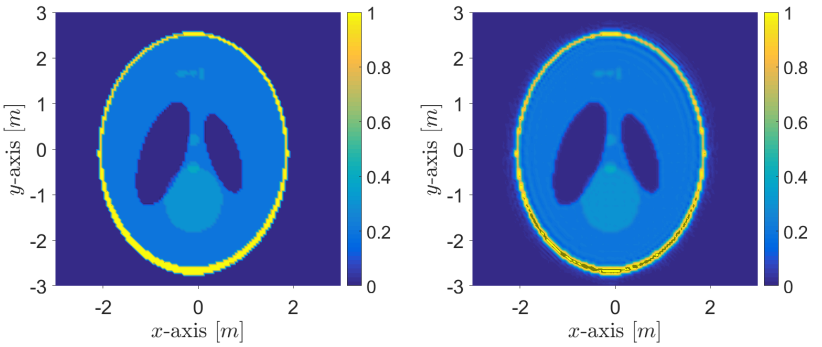


(a) Exact phantom $|\boldsymbol{f}_{\text{ph}}(\boldsymbol{x})|$ (b) Recons. with $g_1(t)$; error: 23.2%

(c) Recons. with $g_2(t)$; error: 13.7% (d) Recons. with $g_3(t)$; error: 4.7%

Figure 3: Exact and reconstructions of $|\boldsymbol{f}_{\text{ph}}(\boldsymbol{x})|$ for waves generated with $\boldsymbol{f}_{\text{ph}}(\boldsymbol{x})g_i(t)$. Relative error in $L^2$-norm.

different sources $\boldsymbol{f}_{\rm ph}(\boldsymbol{x})g_i(t)$ $i \in \{1,2,3\}$. For this experiment, the final time $T$ is 23 $[s]$ and the space and time steps are $h = 0.05$ $[m]$ and $dt = 0.005$ $[s]$, respectively.

Figures 3b, 3c, and 3d show the reconstructions of the space-source term for waves generated with sources $\boldsymbol{f}_{\rm ph}(\boldsymbol{x})g_i(t)$, $i \in \{1,2,3\}$. As it occurred with the results of the experiments perfomed in [19] for acoustic waves, the discontinuous time-source term $g_3(t)$ provides better reconstructions than the other terms.

### *5.2. Three-dimensional reconstructions with complete data*

Here, we show the relative error of reconstruction in $L^2$-norm for 3D simulations in the ideal case (without noise, with geophones located over the entire $\partial\Omega$, and with $T$ being long enough). We simulate 3D elastic waves with a source composed by a smooth space-source term

$$\boldsymbol{f}_{\rm sm}(\boldsymbol{x}) = \frac{\boldsymbol{f}_1(\boldsymbol{x})}{\|\boldsymbol{f}_1(\boldsymbol{x})\|} + 0.7\frac{\boldsymbol{f}_2(\boldsymbol{x})}{\|\boldsymbol{f}_2(\boldsymbol{x})\|}, \tag{18}$$

where $\boldsymbol{f}_1(\boldsymbol{x}) = \exp\left(1 - 2^2\left((x_1+0.5)^2 + (x_2-0.5)^2 + x_3^2\right)\right)$ and $\boldsymbol{f}_2(\boldsymbol{x}) = \exp\left(1 - 2^2\left((x_1-0.5)^2 + (x_2+0.5)^2 + x_3^2\right)\right)$ (see Figure 4a). The three time-source terms are the ones considered in Subsection 5.1. The value of the parameters considered here are: $h = 0.05$ $[m]$, $dt = 0.01$ $[s]$, and $T = 7$ $[s]$. Due to local decay behavior of 3D waves (see Theorem 4) the final time $T$ needed for reconstruction in the 3D case is shorter than in the 2D one.

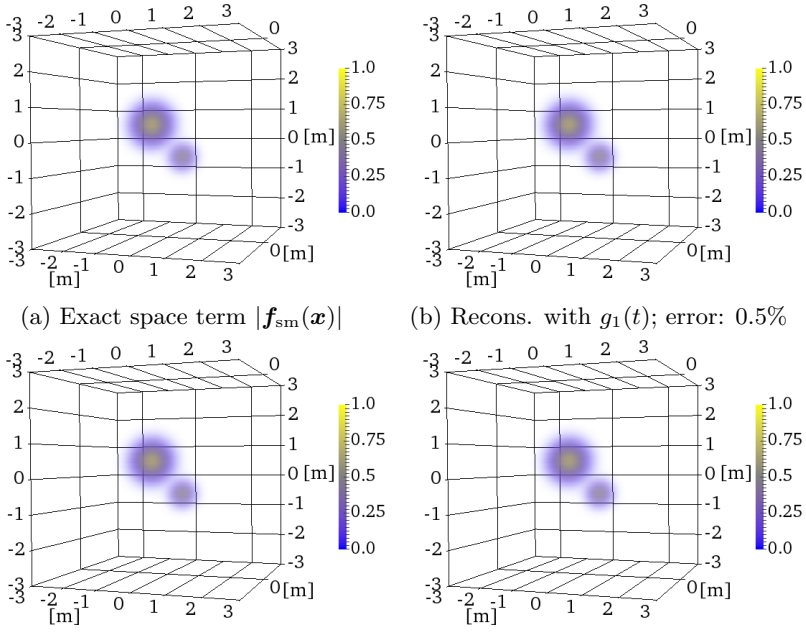

(a) Exact space term $|\boldsymbol{f}_{\rm sm}(\boldsymbol{x})|$ (b) Recons. with $g_1(t)$; error: 0.5%

(c) Recons. with $g_2(t)$; error: 0.6% (d) Recons. with $g_3(t)$; error: 0.6%

Figure 4: Exact and reconstruction of $|\boldsymbol{f}_{\rm sm}(\boldsymbol{x})|$ for waves generated by $\boldsymbol{f}_{\rm sm}(\boldsymbol{x})g_i(t)$. Relative error in $L^2$-norm.

Figures 4b, 4c, and 4d show the reconstructions for the different waves generated with sources $\boldsymbol{f}_{\text{sm}}(\boldsymbol{x})g_i(t)$ for $i \in \{1, 2, 3\}$. The relative errors are lower than those observed in the 2D case for all $g_i(t)$. This is due to the faster local decay rate of 3D waves. In this case (homogeneous media and 3D waves), the Huygens' principle is valid, and we could expect to recover the space-source term exactly. The only two sources of error are the regularization constant $c_0$ and the numerical discretization. In the next experiment, we assess numerically the percent of error induced by the regularization constant $c_0$.

### *5.3. Error decay analysis*

The aim of this numerical experiment is to show numerically the error induced by the regularization constant $c_0$. To do this, we compare the relative error decay in $L^2$-norm between the classical TRM method and the STR with traditional regularization for different $c_0$ constants in 2D and 3D cases. The parameters for the finite difference are: $h = 0.05$ $[m]$, $dt = 0.01$ $[s]$, and $T \in [3, 7]$.

To make the TRM and STR methods comparable, we consider a time-source term acting for a short period of time. Namely, $g_4(t) = 1\chi_{[0,\,0.1]}$. The space-source term selected in this experiment is $\boldsymbol{f}_{\text{sm}}(\boldsymbol{x})$ in (18) and its projection to $\mathbb{R}^2$.

For the classical time reversal method, we consider the problem of reconstructing the initial displacement given by the following inverse problem: find $\boldsymbol{f}_{\text{sm}}(\boldsymbol{x})$ given

$$\begin{cases} \rho\partial_t^2\boldsymbol{u} - L_{\mu,\lambda}\boldsymbol{u} = \boldsymbol{0}, & \text{in } \mathbb{R}^n \times (0,T), \\ \boldsymbol{u}(\boldsymbol{x},0) = \boldsymbol{f}_{\text{sm}}(\boldsymbol{x}), \\ \partial_t\boldsymbol{u}(\boldsymbol{x},0) = \boldsymbol{0}, \end{cases} \tag{19}$$

knowing the measurements $m(\boldsymbol{y},t) = \boldsymbol{u}(\boldsymbol{y},t)$ for all $(\boldsymbol{y},t)$ in $\partial\Omega \times (0,T)$.

For the STR method, we consider the problem of reconstructing the source: given $g_4(t)$ for all $t \in (0,T)$ and the measurements $m(\boldsymbol{y},t) = \partial_t\boldsymbol{u}(\boldsymbol{y},t)$ for all $(\boldsymbol{y},t)$ in $\partial\Omega \times (0,T)$, find $\boldsymbol{f}_{\text{sm}}(\boldsymbol{x})$ such that

$$\begin{cases} \rho\partial_t^2\boldsymbol{u} - L_{\mu,\lambda}\boldsymbol{u} = \boldsymbol{f}_{\text{sm}}(\boldsymbol{x})g_4(t), & \text{in } \mathbb{R}^n \times (0,T), \\ \boldsymbol{u}(\boldsymbol{x},0) = \boldsymbol{0}, \\ \partial_t\boldsymbol{u}(\boldsymbol{x},0) = \boldsymbol{0}. \end{cases} \tag{20}$$

Problems (19) and (20) are different. However, since the time-source term $g_4$ acts only for a short period of time in relation with the total time $T$, we obtain similar wave propagation and errors for both problems, as illustrated in Figure 5. In this way, we can compare the intrinsic error of the TRM and the percent of error due to the STR method. Figure 5 also analyzes the effect of regularization constant $c_0$. In all cases, we observe that such constant has negligible effects on the accuracy of the resulting reconstruction.

### *5.4. Tree-dimensional reconstruction with partial data and noise*

We now analyze the case when only partial boundary data are available and the influence of noise on the partial data. To do this, we present reconstructions of the space-source term $\boldsymbol{f}_{\text{sm}}(\boldsymbol{x})$ (see (18)) when the measurements are obtained in a subset of the domain boundary. We consider three cases. In the first one, geophones are located on

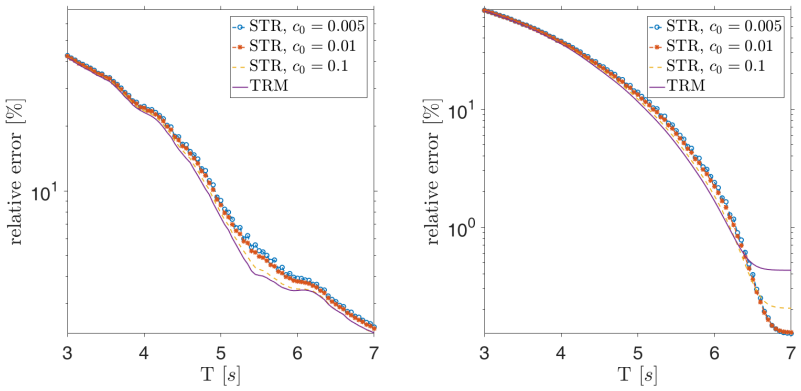


(a) 2D case (b) 3D case

Figure 5: Error decay comparison between TRM and STR for different values of $c_0$.

four faces of the cube $[-3,3]\times[-3,3]\times[-3,3]$; in the second one, geophones are located on two faces of the cube; and in the third case, geophones are located only along one face of the cube. Then, we repeat the last experiment (geophones located along one face) but considering noisy measurements. To pollute the measurements, we added 5% and 10% of white Gaussian noise. The geophones are located at each node of the numeric mesh over $\Gamma_h$, possibly only on some faces of $\partial\Omega$. The value of the finite difference discretization parameters are: $h = 0.05$ $[m]$, $dt = 0.01$ $[s]$, and $T = 7$ $[s]$.

Figure 6 shows the exact source and the respective reconstructions when clean measurements are acquired in four, two, and one faces of the domain boundary. The amplitude of the reconstructed sources is related with the amount of information available on the boundary, then the scale of the reconstructions decrease as the number of measured faces decrease. Although we obtain a smaller scale in the reconstructions with partial boundary information, the STR method with traditional regularization properly localizes the space-source term and reconstructs it with lower resolution.

In Figure 7, we see the reconstruction of the source $\boldsymbol{f}_{\rm sm}(\boldsymbol{x})$, when noisy measurements are acquired on one face of the cube. Subfigures 7a and 7b show the reconstruction with 5% and 10% of noise, respectively. Here, we observe that the noise influence is proportionally scaled as the source reconstruction, and the method is still able to locate the source.

### *5.5. Comparison of two STR regularization methods: traditional vs fast cut-off*

Here, we compare both STR regularization methods for reconstructions performed with data information on the entire boundary and with partial boundary data. To do this, we consider 2D reconstructions of the phantom $\boldsymbol{f}_{\rm ph}(\boldsymbol{x})$ from measurements of generated with $\boldsymbol{f}_{{\rm ph}(\boldsymbol{x})}g_3(t)$ (see Figures 3a and 2c). For each set of reconstructions the measurements are obtained on the entire boundary, on two faces, and on one face of the boundary. For this experiment, the final time $T$ is 23 $[s]$ and the space and time steps are $h = 0.05$ $[m]$ and $dt = 0.005$ $[s]$, respectively.

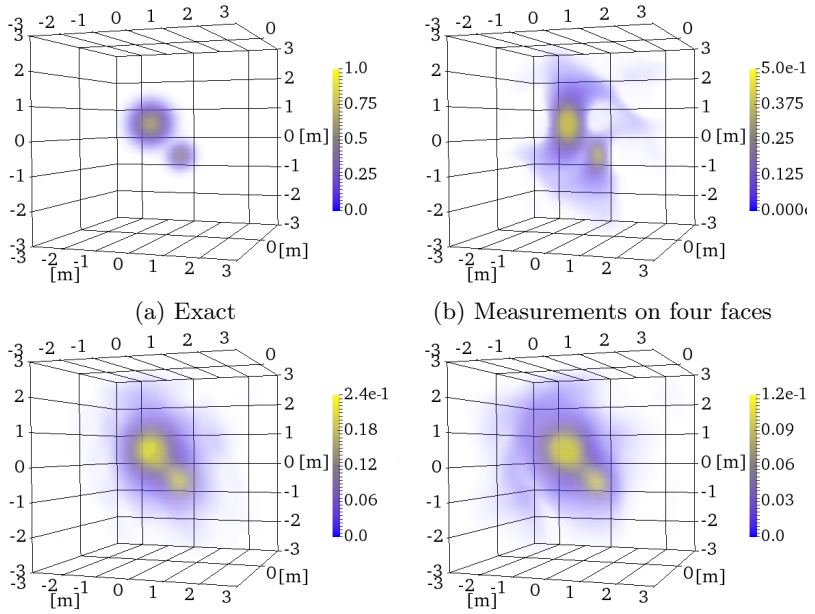


(a) Exact (b) Measurements on four faces

(c) Measurements on two faces (d) Measurements on one face

Figure 6: Exact and reconstruction of $|\boldsymbol{f}_{\mathrm{sm}}(\boldsymbol{x})|$ for waves generated by $\boldsymbol{f}_{\mathrm{sm}}(\boldsymbol{x})g_1(t)$.

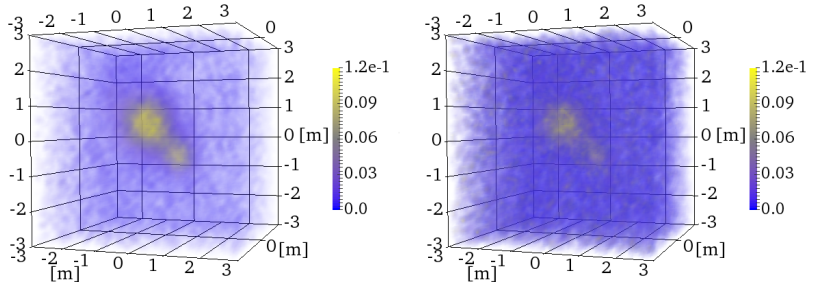


(a) 5% white Gaussian noise (b) 10% white Gaussian noise

Figure 7: Reconstruction of $|\boldsymbol{f}_{\mathrm{sm}}(\boldsymbol{x})|$ for waves generated by $\boldsymbol{f}_{\mathrm{sm}}(\boldsymbol{x})g_1(t)$. Measurements on one face with white Gaussian noise.

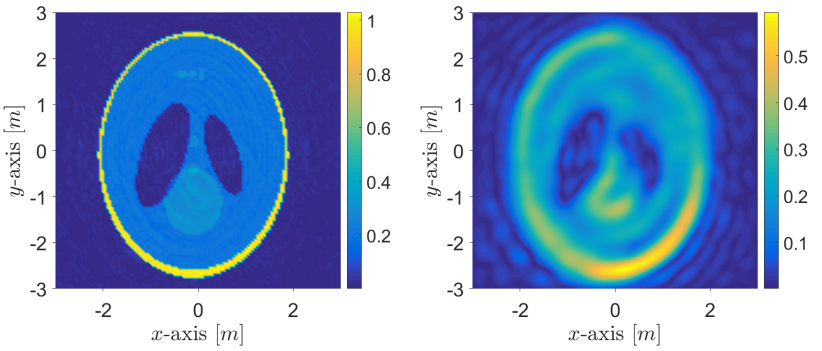


(a) 4 faces; $c_0 = 0.180$; error 7.8%




(b) 4 faces; $c_1 = 0.180$; error 64.9%

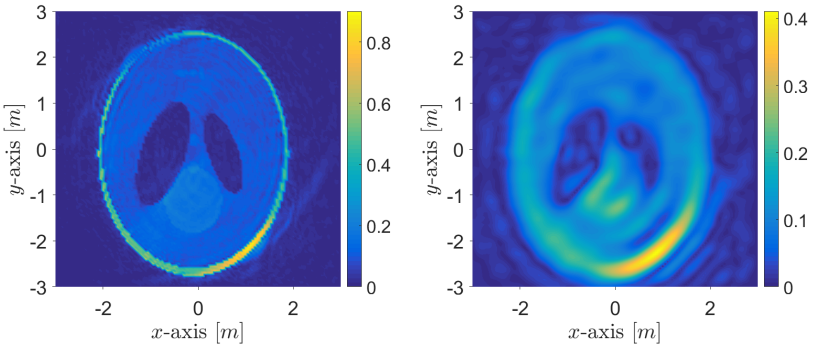


(c) 2 faces; $c_0 = 0.180$; error 50.9%




(d) 2 faces; $c_1 = 0.180$; error 74.7%

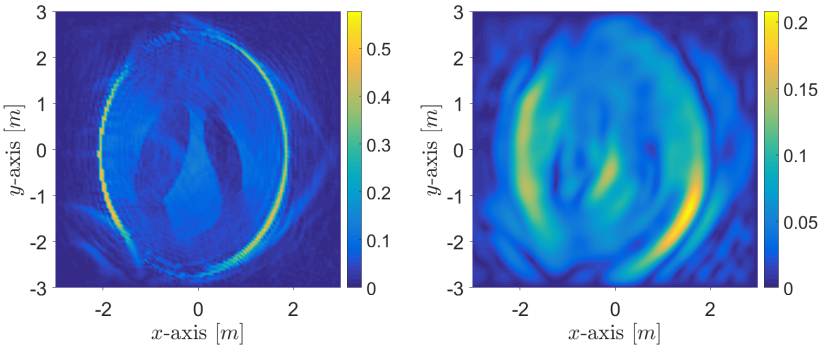


(e) 1 face; $c_0 = 0.180$; error 76.5%




(f) 1 face; $c_1 = 0.180$; error 87.1%

Figure 8: Comparison of STR with traditional regularization ($c_0 = 0.180$) and fast reconstructions with cut-off regularization ($c_1 = 0.180$). Reconstruction of $|\boldsymbol{f}_{\text{ph}}(\boldsymbol{x})|$ with partial data for waves generated with $\boldsymbol{f}_{\text{ph}}(\boldsymbol{x})g_3(t)$. Relative error in $L^2$-norm.

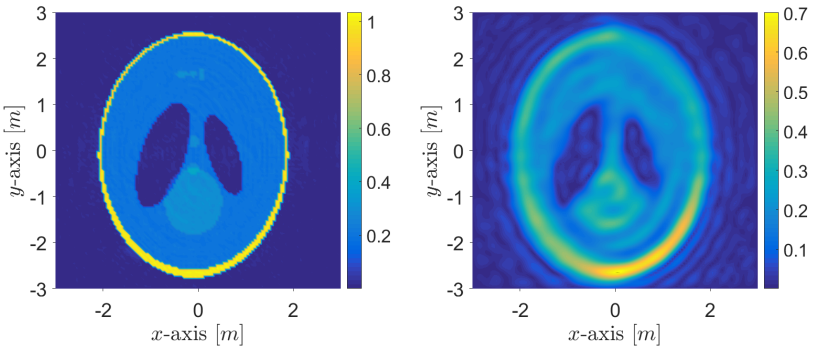


(a) 4 faces; $c_0 = 0.048$; error 5.6%




(b) 4 faces; $c_1 = 0.048$; error 61.6%

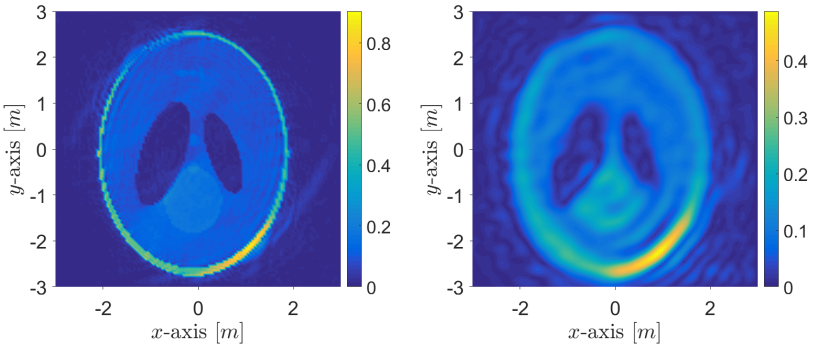


(c) 2 faces; $c_0 = 0.048$; error 50.5%




(d) 2 faces; $c_1 = 0.048$; error 72.5%

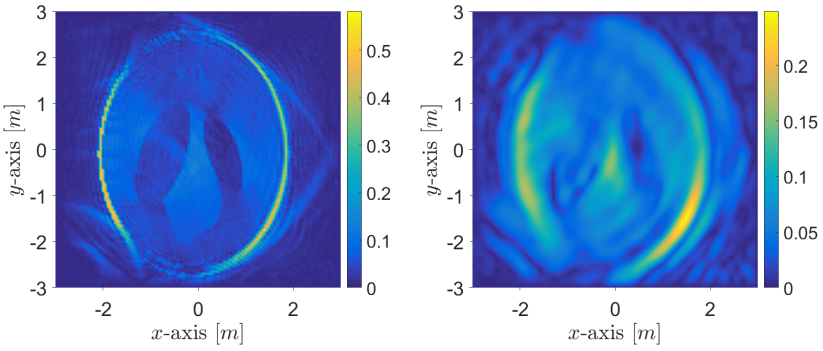


(e) 1 face; $c_0 = 0.048$; error 76.4%




(f) 1 face; $c_1 = 0.048$; error 86.2%

Figure 9: Comparison of STR with traditional regularization ($c_0 = 0.048$) and fast reconstructions with cut-off regularization ($c_1 = 0.048$). Reconstruction of $|\boldsymbol{f}_{\text{ph}}(\boldsymbol{x})|$ with partial data for waves generated with $\boldsymbol{f}_{\text{ph}}(\boldsymbol{x})g_3(t)$. Relative error in $L^2$-norm.

Let $f_{meas}$ be the maximum measured frequency and $f_{STR}$ be the maximum frequency of the signal processed with the STR method. For this comparison, we consider the regularization constant $c_1 = 0.180$, which gives us that $f_{STR} \leq f_{meas}$ for the fast STR with cut-off regularization. Additionally, we consider the case $c_1 = 0.048$, which gives us that $f_{STR} \leq 2f_{meas}$. To compare the methods, we consider the same regularization constants values for the STR with traditional regularization, but in this case the method induces higher frequencies.

Figures 8 and 9 show the reconstruction images for the different boundary information considered. The subfigures are intentionally on different scale for a better understanding of the results. The STR with traditional regularization presents a lower error percent in all cases and identifies better the edges of the phantom. Although the fast STR with cut-off regularization loses some "details" in the reconstruction when $f_{STR} \leq f_{meas}$ (and $f_{STR} \leq 2f_{meas}$), the methodology still identifies the correct location of the source and its main structure.

## 6. Numerical experiments of fast STR with cut-off regularization

In this section, we consider a seismicity induced by mining example in 2D using a FEM with a second-order polynomial space discretization (i.e. $p = 2$). We select a regular square grid, and the geophones are located at each nodal point of $\partial\Omega_h$. For a more realistic implementation, we pollute P- and S-waves synthetic measurements with additive Gaussian noise. To reconstruct the source, we implement the fast STR method by solving problem (12) and replacing operator $\mathcal{A}_0$ with the transformed data given by equation (14).

For these experiments, we generate a microseismic event considering three point sources acting simultaneously and modulated by a Ricker wavelet on time. These sources are located at points $(170, -135)$, $(0, -10)$, and $(140, 160)$, where the units are now in meters. Geophones are distributed ten meters away along the boundary of the set $\Omega = (-300, 300)\times(-300, 300)$. We consider $\rho = 2500$ $[Kg/m^3]$, $\mu = 9.6334225\times10^9$ $[Pa]$, $\lambda = 9.633155 \times 10^9$ $[Pa]$. Thus, $v_p = \sqrt{(2\mu + \lambda)/\rho} = 3400$ $[m/s]$ and $v_s = \sqrt{\mu/\rho} = 1963$ $[m/s]$, so $v_p/v_s \approx \sqrt{3}$. The case when $v_p/v_s$ is $\sqrt{3}$ is considered close to the real conditions for much of the Earth [2].

In addition, we set the cut-off constant $c_1 = 0.01$ to compute the fast STR method. For the computational mesh, we select $h = 10$ $[m]$, $dt = 0.001$ $[s]$, and $T = 0.6$ $[s]$.

Figure 10 shows the results of the source reconstructions where the measurements are acquired in presence of additive noise. In all cases, we observe superior reconstruction results.

## 7. Conclusions

We have developed a space-source term reconstruction method in linear elasticity for sources of the form $\boldsymbol{f}(\boldsymbol{x})g(t)$. The proposed method is based on the STR methodology introduced in [19] for acoustic waves. Additionally, we describe two regularization methods: a traditional one, and a fast cut-off regularization.

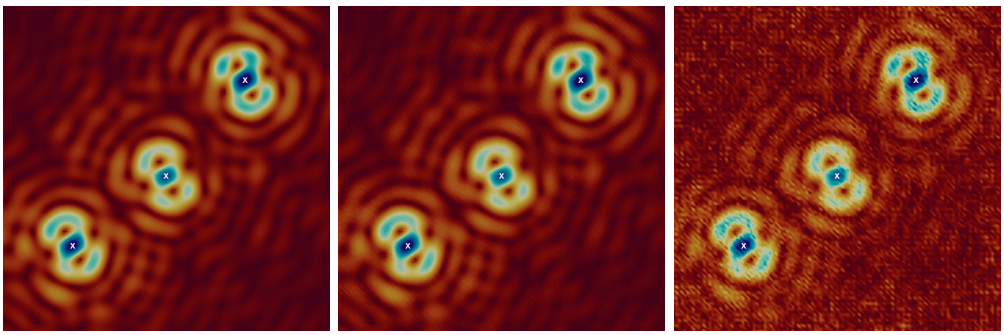

(a) without noise (b) noise: 10% (c) noise: 30%

Figure 10: Source reconstruction of seismicity induced by mining experiment from measurements with different percent of additive noise. The white crosses represent the exact position of the original point source.

The STR method has its basis on a property that allows waves to be reversed in time and the Duhamel's principle to define an auxiliary problem without source and with final conditions. Additionally, the STR method requires a non-trapping condition to ensure the wavefronts measurements and a local decay result to approximate by zero the final conditions of the auxiliary problem given by the Duhamel's principle. A Volterra integral equation of the first kind with a convolution kernel gives the relation between the boundary measurements of the physical and the auxiliary problems. To reverse in time the boundary information in the auxiliary problem, it is necessary to solve the Volterra equation. Here, we have developed the two regularization methods mentioned above to solve such Volterra equation.

We have performed numerical experiments in 2D and 3D to test the reconstruction method with both regularization approaches. The STR method with traditional regularization considers a regularization constant $c_0$ to avoid divisions by zero. This methodology works well with partial data but excites some high-frequencies that require a fine mesh in space to backpropagate them. The fast STR method with cut-off regularization introduces a cut-off constant $c_1$ as a low-pass filter to avoid the higher frequencies in the processed measurements. The fast method works well under noise measurements and with coarser meshes but presents some reconstruction limitations in the case with partial data. Additionally, 3D simulations exhibit a better local decay rate, which is traduced into better source reconstructions at shorter times.

In a future work, we shall extend the STR methodology to heterogeneous elastic materials. Heterogeneous media allows a more accurate description of the ground and a better representation of the different layers that compose the Earth. Since the TRM method is suitable also for heterogeneous media (see [35]), the STR methodology should also be applicable if the media accomplishes a non-trapping condition. Additionally, we plan to study a theoretical estimate of the reconstruction error in the elastic case.

## Acknowledgments

This work was partially supported by the European Union's Horizon 2020 research and innovation programme under the Marie Sklodowska-Curie grant No 644602 GEAGAM and CONICYT - PIA/Concurso de Apoyo a Centros Cient´ıficos y Tecnol´ogicos de Excelencia con Financiamiento Basal AFB170001. Additionally, the first author was supported by CONICYT Doctoral fellowship number 21120646, Fondecyt 11161033, ICM P09-015-F, and EQM140119. Jaime H. Ortega was partially supported by Fondecyt 1111012 and 1171854. Ángel Rodríguez-Rozas and David Pardo were partially funded by the Projects of the Spanish Ministry of Economy and Competitiveness with reference MTM2016-76329-R (AEI/FEDER, EU) and MTM2016-81697-ERC/AEI, the BCAM "Severo Ochoa" accreditation of excellence SEV-2013-0323, the Basque Government through the BERC 2014-2017 program, the Consolidated Research Group Grant IT649-13 on "Mathematical Modeling, Simulation, and Industrial Applications (M2SI)". David Pardo has also received funding from the European Union's Horizon 2020 research and innovation programme under the Marie Sklodowska-Curie grant agreement No 777778.

## References

[1] K. Aki, P. G. Richars, Quantitative seismology, 2nd Edition, University Science Books, 2002.

[2] S. J. Gibowicz, A. Kijko, An introduction to mining seismology, Academic Press, 1994.

[3] M. S. Hons, R. R. Stewart, D. C. Lawton, M. B. Bertram, G. Hauer, Field data comparisons of mems accelerometers and analog geophones, The Leading Edge 27 (2008) 896–903. doi:10.1190/1.2954030.

[4] V. Isakov, Inverse source problems, American Mathematical Society, Providence, 1990.

[5] M. Yamamoto, Stability, reconstruction formula and regularization for an inverse source hyperbolic problem by a control method, Inverse Problems 11 (1995) 481–496. doi:10.1088/0266-5611/11/2/013.

[6] G. C. Garcia, A. Osses, M. Tapia, A heat source reconstruction formula from single internal measurements using a family of null controls, Journal of Inverse and Ill-posed Problems 21 (2013) 755–779. doi:10.1515/jip-2011-0001.

[7] A. E. Badia, T. Ha-Duong, An inverse source problem in potential analysis, Inverse Problems 16 (2000) 651–663. doi:10.1088/0266-5611/16/3/308.

[8] A. E. Badia, T. Ha-Duong, F. Moutazaim, Numerical solution for the identification of source terms from boundary measurements, Inverse Problems in Engineering 8 (2000) 345–364. doi:10.1016/j.apm.2012.03.024.

[9] H. Ammari(Ed.), Mathematical modeling in biomedical imaging I: Electrical and ultrasound tomographies, anomaly detection, and brain imaging, Springer, Berlin, 2009. doi:10.1007/978-3-642-03444-2.

[10] M. Fink, C. Prada, F. Wu, D. Cassereau, Self focusing in inhomogeneous media with time reversal acoustic mirrors, Proceedings., IEEE Ultrasonics Symposium 2 (1989) 681–686. doi:10.1109/ULTSYM.1989.67072.

[11] M. Fink, D. Cassereau, A. Derode, C. Prada, P. Roux, M. Tanter, J.-L. Thomas, F. Wu, Time-reversed acoustics, Reports on Progress in Physics 63 (2000) 1933–1995. doi:10.1088/0034-4885/63/12/202.

[12] H. Ammari, An introduction to mathematics of emerging biomedical imaging, Springer, Berlin, 2008. doi:10.1007/978-3-540-79553-7.

[13] H. Ammari, E. Bretin, J. Garnier, W. Jing, H. Kang, A. Wahab, Localization, stability, and resolution of topological derivative based imaging functionals in elasticity, SIAM Journal on Imaging Sciences 6 (2013) 2174–2212. doi:10.1137/120899303.

[14] J. Yoo, Y. Jung, M. Lim, J. Ye, A. Wahab, A joint sparse recovery framework for accurate reconstruction of inclusions in elastic media, SIAM Journal on Imaging Sciences 10 (2017) 1104–1138. doi:10.1137/16M110318X.

[15] H. Ammari, E. Bretin, J. Garnier, A. Wahab, Time reversal in attenuating acoustic media, Contemporary Mathematics 548 (2011) 151–163. doi:10.1090/conm/548/10841.

[16] H. Ammari, J. Garnier, W. Jing, H. Kang, M. Lim, K. Sølna, H. Wang, Mathematical and statistical methods for multistatic imaging, Springer, 2013. doi:10.1007/978-3-319-02585-8.

[17] H. Ammari, E. Bretin, J. Garnier, H. Kang, H. Lee, A. Wahab, Mathematical methods in elasticity imaging, Princeton University Press, 2015. doi:10.2307/j.ctt1287kr2.

[18] H. Ammari, E. Bretin, J. Garnier, A. Wahab, Noise source localization in an attenuating medium, SIAM Journal on Applied Mathematics 72 (2012) 317–336. doi:10.1137/11083191X.

[19] R. I. Brevis, J. H. Ortega, D. Pardo, A source time reversal method for seismicity induced by mining, Inverse Problems and Imaging 11 (2017) 25–45. doi:10.3934/ipi.2017002.

[20] P. L. Gould, Introduction to linear elasticity, Springer, New York, 2013. doi:10.1007/978-1-4614-4833-4.

[21] M. R. Eslami, R. B. Hetnarski, J. Ignaczak, N. Noda, N. Sumi, Y. Tanigawa, Theory of elasticity and thermal stresses, Springer, Dordrecht, 2013. doi:10.1007/978-94-007-6356-2.

[22] G. Lamé, Leçons sur la théorie mathématique de l'elasticité des corps solides, Gauthier-Villars, 1852.

[23] E. Deriaz, V. Perrier, Orthogonal helmholtz decomposition in arbitrary dimension using divergence-free and curl-free wavelets, Applied and Computational Harmonic Analysis 26 (2009) 249–269. doi:10.1016/j.acha.2008.06.001.

[24] A. Chorin, J. E. Marsden, A mathematical introduction to fluid mechanics, 3rd Edition, Springer, New York, 1993. doi:10.1007/978-1-4612-0883-9.

[25] V. Girault, P. A. Raviart, Finite element methods for Navier-Stokes Equations, Springer, Berlin, 1986. doi:10.1007/978-3-642-61623-5.

[26] B. R. Vainberg, On the short wave asymptotic behaviour of solutions of stationary problems and the asymptotic behaviour as $t \to \infty$ of solutions of non-stationary problems, Russian Mathematical Surveys 30 (1975) 1–58. doi:10.1070/RM1975v030n02ABEH001406.

[27] Y. V. Egorov, M. A. Shubin, Foundations of the classical theory of partial differential equations, Springer, Berlin, 1998. doi:10.1007/978-3-642-58093-2.

[28] M. Fink, Time-reversal mirrors, Journal of Physics D: Applied Physics 26 (1993) 1333–1350. doi:10.1088/0022-3727/26/9/001.

[29] P. Cance, Y. Capdeville, Validity of the acoustic approximation for elastic waves in heterogeneous media, Geophysics 80 (2015) T161–T173. doi:10.1190/geo2014-0397.1.

[30] L. Evans, Partial differential equations, 2nd Edition, American Mathematical Society, Providence, 2010. doi:10.1090/gsm/019.

[31] P. Linz, Analytical and numerical methods for Volterra equations, Society for Industrial and Applied Mathematics, Philadelphia, 1985. doi:10.1137/1.9781611970852.

[32] K. R. Kelly, R. W. Ward, S. Treitel, R. M. Alford, Synthetic seismograms: a finite-difference approach, Geophysics 41 (1976) 2–27. doi:10.1190/1.1440605.

[33] A. Rodríguez-Rozas, J. Diaz, Non-conforming curved finite element schemes for time-dependent elastic–acoustic coupled problems, Journal of Computational Physics 305 (2016) 44–62. doi:10.1016/j.jcp.2015.10.028.

[34] L. A. Sheep, B. F. Logan, The Fourier reconstruction of a head section, IEEE Transactions on Nuclear Science 21 (1974) 21–43. doi:10.1109/TNS.1974.6499235.

[35] P. D. Norville, W. R. Scott Jr., Time-reversal focusing of elastic surface waves, The Journal of the Acoustical Society of America 118 (2005) 735–744. doi:10.1121/1.1945468.